EXPLORING CENTRIN TARGETS: KRR1, AND THE CENTRIN-SFI1$_{P21}$ COMPLEX SALT-BRIDGE INTERACTION

by

Ruth R. Almodóvar Pérez

A thesis submitted in partial fulfillment of the requirements for the degree of

MASTER OF SCIENCE
in
CHEMISTRY

UNIVERSITY OF PUERTO RICO
MAYAGÜEZ CAMPUS
2015
Approved by:

_____	_____
Nilka Rivera Portalatin, Ph.D. Member, Graduate Committee	Date
_____	_____
María A. Aponte Huertas, Ph.D. Member, Graduate Committee	Date
_____	_____
Belinda Pastrana Ríos, Ph.D. President, Graduate Committee	Date
_____	_____
Madeline Torres, Ph.D. Representative of Graduate Studies	Date
_____	_____
Aidalú Joubert, Ph.D. Chairperson of the Department	Date

ABSTRACT

Centrins are small calcium binding proteins and ubiquitous centrosome components. Centrins play a fundamental role in the structure and function of centrioles, basal bodies, primary cilia and the microtubule-organizing center of lower eukaryotes. In humans, four centrin isoforms have been identified (*Hs*cen1, *Hs*cen2, *Hs*cen3, and *Hs*cen4). The structure of these small proteins is comprised of two rounded domains containing two EF-hands and tethered by a helix. The EF-hands act as calcium sensors within cells. The particularity of centrin's structure provides the ability to refine interactions with numerous biological targets. In this study, we explore two centrin targets. First the expression and purification of the novel protein Krr1 was established. Krr1 is a human processome subunit that co-localizes with *Hs*cen2 in the nucleus. Krr1 is known to be involved in ribosome biogenesis and RNA processing, nevertheless information regarding Krr1 is limited and human Krr1 research remains a novel area of study. Secondly the complex formation between *Hs*cen1 and human Sfi1 was examined. Human Sfi1 is one of the centrin biological targets that co-localizes to centrioles and basal bodies. The aim was to study the existence of a potential salt bridge interaction between human centrin and Sfi1p. Using two dimensional infrared (2D IR) correlation spectroscopy and the labeled isotope $^{15}N_2$-Arg_{16}*Hs_Sfi1*p_{21} we were able to establish unequivocally the existence of this key salt-bridge interaction, crucial to elucidating the mechanism of complex formation and the role of the bridge interaction within the *Hs*cen1-$^{15}N_2$-Arg_{16}*Hs_Sfi1*p_{21} complex.

RESUMEN

Las centrins son proteínas que enlazan calcio y componentes ubicuos del centrosoma. Estas juegan un papel fundamental en la estructura y función de los centriolos, cuerpos basales, cilia primaria y el centro organizador de microtubos en células eucariotas inferiores. En humanos, hay cuatro isoformas de centrin identificadas (*Hs*cen1, *Hs*cen2, *Hs*cen3, and *Hs*cen4). La estructura de estas proteínas se compone de dos dominios globulares que contienen dos manos-EF y están unidos por una hélice. Las manos-EF actúan como sensores de calcio dentro de las células. Esta estructura particular le provee a centrin la habilidad de refinar interacciones con múltiples proteínas enlazantes. En este estudio, se exploran dos proteínas enlazantes a centrin. Primeramente se establece la expresión y purificación de la proteína novel humana Krr1 que forma parte del proceosoma y está colocalizada con *Hs*cen2 al núcleo. Krr1 está involucrada en la biogénesis del ribosoma y el procesamiento del ARN. Sin embargo, dada la escasez de estudios de esta proteína, Krr1 permanece como un área innovadora de estudio. Finalmente se examina la formación del complejo entre *Hs*cen1 y la proteína humana Sfi1. Sfi1 humana es una proteína enlazante a centrin que se encuentra co-localizada en centriolos y cuerpos basales. El objetivo fue caracterizar la formación del complejo humano centrin-Sfi1 examinando la interacción en un puente salino entre *Hs*cen1 y *Hs_Sfi1*. Por medio de la espectroscopía infrarroja de correlación en dos dimensiones (2D IR, según sus siglas en inglés) y el isótopo marcado $^{15}N_2$-Arg_{16}*Hs_Sfi1*p_{21}, se logró establecer, sin lugar a duda, la existencia de interacción por medio de un puente salino, a la misma vez que su rol en el mecanismo de la formación del complejo *Hs*cen1-$^{15}N_2$-Arg_{16}*Hs_Sfi1*p_{21}.

DEDICATION

I want to dedicate this thesis to my family: my father, Luis, who always encouraged me to continue studying, despite the multiple challenges of this career; to my mother, Ruth, who gave me support and lovingly listened to me when I needed a pep talk, to my sister Roxanne Marie and my brother Luis Angel for their great love and unconditional support throughout the years.

Finally, this thesis is dedicated to all of my extended family, who has unfailingly provided me with emotional, intellectual and spiritual nourishment and support.

AKNOWLEDGEMENTS

First, a special thanks to Dr. Belinda Pastrana, Chair of my Committee, for the great opportunity given by accepting me as part of her research group. Her ample knowledge and mentoring throughout the entire project was always there for me. Dr. Pastrana has always been a great source of support with her infectious passion for scientific research. I thank you for the countless hours spent prodding me toward the successful completion of my thesis, always with patience, discipline and honesty.

I would also like to thank the members of my graduate committee, Dr. Nilka Rivera Portalatin and Dr. María Aponte Huertas, for their support and recommendations.

I want to acknowledge several people who have been of great help to me, without even knowing it. Thanks go out to the great research team of Q-307 and Q-309, undergraduate and graduate students alike, but especially to Ana María Gómez and Daniel Narváez, for their counseling at each step of the process. Exceptional thanks go to Marie Cely Rosado and Adalberto Díaz for their unconditional friendship and company.

Special thanks go to my family: Mom, Dad, Roxy and Luiggy for being a constant source of love and support in my life.

TABLE OF CONTENTS

LIST OF FIGURES

1. INTRODUCTION

The study of novel targets and, subsequently their interactions with well-known proteins, helps in the overall understanding of cellular networks. For the novel centrin target Krr1, little is known about the protein, it's interactions with surrounding proteins and the implications of its existing KH domain. Its interaction with centrin was identified through yeast-two-hybrid assay (Dr. Walter Chazin personal communication). The amino acid sequence of Krr1 was examined, compared to known centrin targets, and identified a potential centrin binding site. In order to explore this putative centrin-Krr1 interaction, we chose to clone and express a recombinant Krr1 target.

Another known centrin target is the Sfi1 protein. These human proteins have equally interacting counterparts in other organisms such as the well-studied yeast spindle pole body. The centrin-Sfi1p complex has been biologically confirmed by its co-localization to the centrioles[1]. X-ray crystal structure of the complex has also been determined[2] in *Saccharomyces cerevisiae* with Cdc31, a centrin homologue. Yet, important questions remain as to the stability and mechanism of centrin-Sfi1p complex formation, such as: elucidating the existence of a salt-bridge interaction and the potential role this salt-bridge may have on complex formation and its implications in centriole assembly and function.

Revealing the effect of these proteins in a much larger scale of events such as primary cilia function and its relationship with disease states, such as cancer[3] is central in the

design of therapeutics. As such, the importance of elucidating target binding mechanisms cannot be understated.

The work presented in this study aims to help provide answers to some of the questions regarding the interaction between *Hs*_cen1 and *Hs*_Sfi1 by evaluating the complex via Fourier Transformed Infrared (FT-IR) Spectroscopy.

Few techniques are as useful at revealing protein-protein interactions (PPI'S) on the molecular level as two-dimensional infrared (2D IR) correlation spectroscopy. Our group has a long track record of effectively applying 2DCOS to the study of proteins and PPI's. Furthermore, we have proven 2D IR correlation spectroscopy in the study of temperature-induced conformational changes, aggregation process, and denaturation of proteins is prevalent in the literature[4,36,37,59] allowing for further contribution towards the clarification of various pathways. This investigation takes advantage of these methods to further reveal the nature of the interaction between centrin and Sfi1.

1.1 Objectives

The primary goals of this study are to generate a pure recombinant Krr1 that can be biochemically characterized, as well as to study the interaction between *Hs*_cen1 and *Hs*_Sfi1 via 2D IR correlation spectroscopy. The information derived from both these efforts is key to understanding the effect of these proteins in a much larger scale of events such as disease and cancer, and is central in the design of therapeutics. With that in mind, the following are the proposed objectives concerning this study:

- To Generate the Krr1 recombinant
- To bacterially express Krr1 in a fermentor
- To establish a purification protocol for Krr1
- To establish the existence of a key salt-bridge interaction via 2D IR correlation spectroscopy

2. LITERATURE REVIEW

2.1 Centrosome and Centrioles

Centrosomes are small organelles essential for animal development. Centrosomes have the ability to nucleate and organize the growth of microtubules[5]; as such they are the primary microtubule organizing centers (MTOC) within animal cells. These organelles play a major role in genome stability[6] and cell cycle progression, as well as regulate cell motility, adhesion and polarity in interphase, and enable the organization of the spindle poles during mitosis[7]. Similar structures can be found in many organisms, including the spindle pole body[8] (SPB) in model organism *Saccharomyces cerevisiae* (Figure 1). These complex microtubule-based structures have been found analogous in their arrangement to basal bodies required for cilia and flagella[9].

The centrosome is not bound by any membrane. In mammals, it is arranged in the form of a pair of centrioles embedded in a matrix of proteins known as the pericentriolar material (PCM). This PCM contains proteins that are responsible for microtubule nucleation and anchoring such as γ-tubulin, pericentrin and ninein, as well as proteins that have been habitually associated with disease, for example BBS4[10] (Bardet-Biedl syndrome 4 protein).

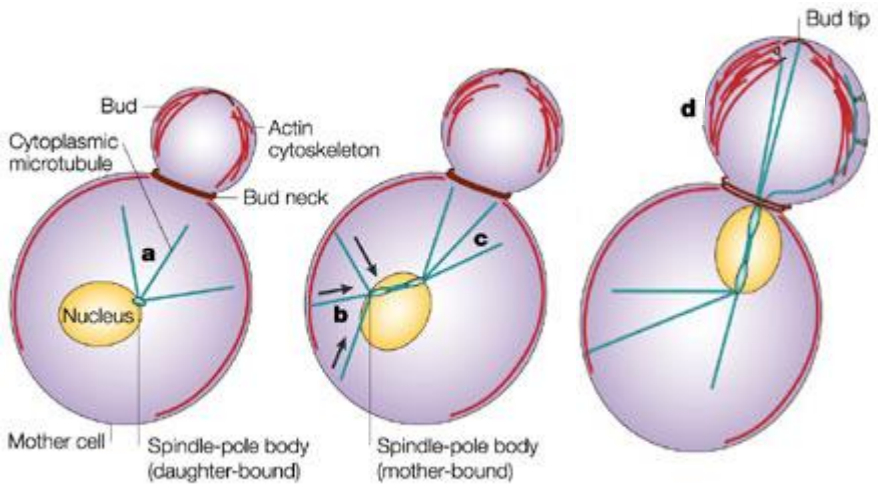

Figure 1. Example of Spindle Pole Body in budding yeast

For the spindle to be positioned at the pre-defined site of cell division, dynamic microtubules use cortical cues and forces at the bud neck. (a) Dynamic microtubules that are nucleated from the bud-bound spindle-pole body undergo dynamic instability to search the cytoplasmic space, to find and capture the bud neck. (b) Forces (arrows) from the opposing, mother-cell-bound spindle-pole body help to push the spindle towards the bud neck. (c) Dynamic microtubules are captured and stabilized by attachment to the bud neck. (d) Microtubule attachment to the bud-tip or the mating-projection. Bud attachment and proper spindle positioning are necessary for equal segregation of the genome to mother and daughter cells. [Adapted from Pearson and Bloom, 2004][11]

A pair of centrioles is divided into a mother and a daughter centriole. The mother centriole has an important role in centriole duplication[12], serving as the template and anchor for the production of a daughter centriole (also known as procentrioles before they achieve their full length). In the form of basal bodies, the mother centriole is critical for the development of the primary and secondary cilium in differentiated cells[13].

Centrioles separate and duplicate once during the cell cycle as a pre-requisite step during cell division. They present two pathways of replication: normal centriole cycle, wherein the daughter centriole buds from the proximal end of the mother centriole, and the *de novo* pathway, where centrioles form without any centrioles previously present in the cell. However, the assembly of centrioles *de novo* is inhibited by the presence of a single centriole. Four consecutive steps have been described[14] in a normal centriole cycle: centriole disengagement, nucleation of the daughter centrioles (procentrioles), elongation of the procentrioles and separation of the centrosomes.

The centriole can be structurally described as having a cylindrical array of nine sets of triplet microtubules, defined by a nine-fold symmetry. There is a region close to the base (proximal end) of the daughter centriole, known as the transition zone (Tz) where a unique structure is comprised of stellate fibers. This cylindrical array forms a distinctive cartwheel structure (Figure 2A,C). At the distal end the triplet microtubules are reduced to doublets. Some of these fibers comprised of Sfi1 and enriched for centrin act as calcium sensitive contractile fibers, between the microtubules within the transition zone[15,16]. Of these, centrin has been shown to be necessary for centriole formation in human cells[17]. The Tz varies in structure, and molecular organization among different organisms. It is usually found at the base of cilium. These structures in

the form of basal bodies are crucial for the formation of flagella and cilia. In recent years, many human proteins associated with disease and cancer were discovered to localize to the Tz[18,19] raising important questions about its assembly and function.

It has long been proposed that a causal link exists between the number of centrioles and human cancer[8], as well as evidence of tumorgenesis in other organisms[20]. However, the relationship between centriole structure and disease remains enigmatic.[21,22] Until recently, little information was known about the centriole to basal body transition[23].The characterization of the molecular components of basal bodies and specifically the mother centriole can be expected to provide a better understanding of the biogenesis of these structures.

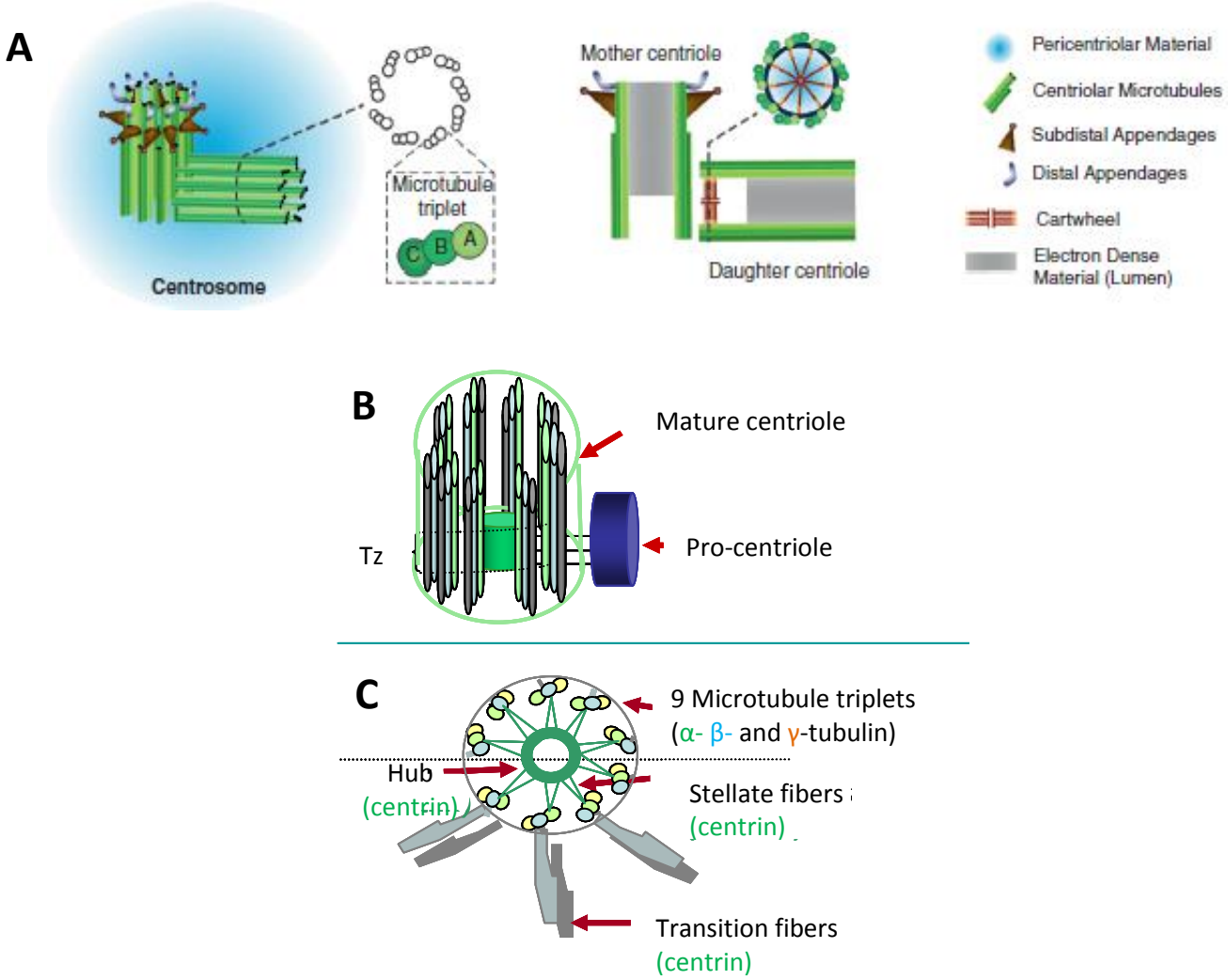

Figure 2. Structure of a vertebrate centrosome and description of its components

The centrosome is the major microtubule-organizing center of most animal cells. A centrosome (A) is formed by two cylinder-shaped microtubule-based structures, the centrioles, which are surrounded by a protein matrix cloud, the pericentriolar material (PCM). Each centrosome is composed of a mature (mother) and an immature (daughter) pro-centriole, shown in B and C as follows: Centriole and pro-centriole in orthogonal arrangement (B), transverse cut at transition zone (Tz): transition zone during S phase (C) of the cell cycle. Basal bodies are homologous structures, in that they have similar Tz with microtubule doublets instead of triplets. [Adapted from Bettencourt-Dias and Glover[7], 2007]

2.2 Centrin

Centrins are small calcium binding proteins (CaBP) that are ubiquitous centrosome components[24]. Centrin is a known signature eukaryotic protein[25] of which there is no significant homolog in bacteria or Archaea. This CaBP is essential for the initial phase of centriole/basal body/spindle pole body assembly in mammals, *Chlamydomonas reinhardtii* and yeast respectively, whether by the use of a template or de novo pathways. Centrins play a fundamental role in microtubule-organizing center structure and function, and are requisite for the duplication of centrioles[25] and formation of basal bodies[26]. In more recent years, this protein has also been found to be localized to the nucleus[27]. Centrin is found in many organisms; however there are four known isoforms in higher eukaryotes with different and occasionally interchangeable biological functions. These four isoforms are centrin 1, centrin 2, centrin 3 and centrin 4. Three of the centrin isoforms are found in humans (*Hs*cen1, *Hs*cen2, *Hs*cen3), while centrin 4 is found in mice. Human centrin 1 is found in male germ cells[28] and retina[29], human centrin 2 is localized to the nucleus and is a structural component of centrioles along with human centrin 3. *Hs*cen2 is also involved in global genome nucleotide excision repair[30,31]. Lastly, though the role of centrin 4 is lesser known, this protein has been found localized to ciliated cells inside the brains of mice[32, 33].

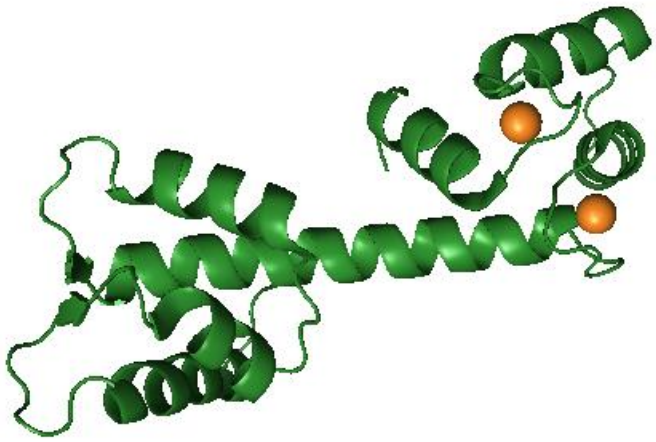

Figure 3. Centrin structure with calcium binding sites occupied (PDB ID: 2GGM[31])

In this structure, Human centrin 2 binds to two calcium ions via its calcium binding sites on the C-terminus of the protein. Centrin has four helix-loop-helix motifs known as EF hands, capable of binding calcium. However, only four full-length centrin protein complexes have been resolved to date: Cdc31-SFi1 complex[2] (2DOQ), CdC31-Sus-Sac3[34] (3FWC) complex, Crcen-MLT[35] complex (3QRX) and the Hscen2-XPC (2GGM) depicted above.

The thermodynamics of centrin and many of its isoforms have been studied exhaustively. Centrins are small dumbbell shaped proteins that have 167-172 amino acids (Figure 3). Structurally, centrins form part of the EF-hand superfamily, which is the archetypal metal ion binding helix-loop-helix motif. Each isoform of centrin has distinct calcium binding sites, therefore providing slightly different target binding capabilities. Individual centrin function, and it's relation to calcium binding has been previously studied[36] . However, it is only recently that a comprehensive comparative study of the protein stability of the different human centrin isoforms and its relationship calcium binding has been published[37].

Centrin has several biological targets within the centriole and basal bodies (Sfi19, Sac3, Sus1, and POC5) and in the nucleus[31] (XPC, Sumo). Recently, the presence of *Hs*cen1 has been found to be a potential biomarker for pancreatic and prostate cancer[3]. Figure 4 shows an example of the mRNA and protein expression levels in testis, prostrate and pancreas. Centrin1 mRNA expression levels in normal testis remains high when compared to diseased tissue (Figure 4A). However, this relationship is reversed when observing centrin1 levels in prostrate and pancreatic cancer (Figure 4B and Figure 4C), suggesting this protein may be important in studying cancer regulation dynamics.

The role of centrin in centriole duplication remains unclear[38]. A better understanding of the evolution of centrins and their binding proteins will be important to clarify their role in the process of centrosome biogenesis[39] as well as their possible involvement in cancer.

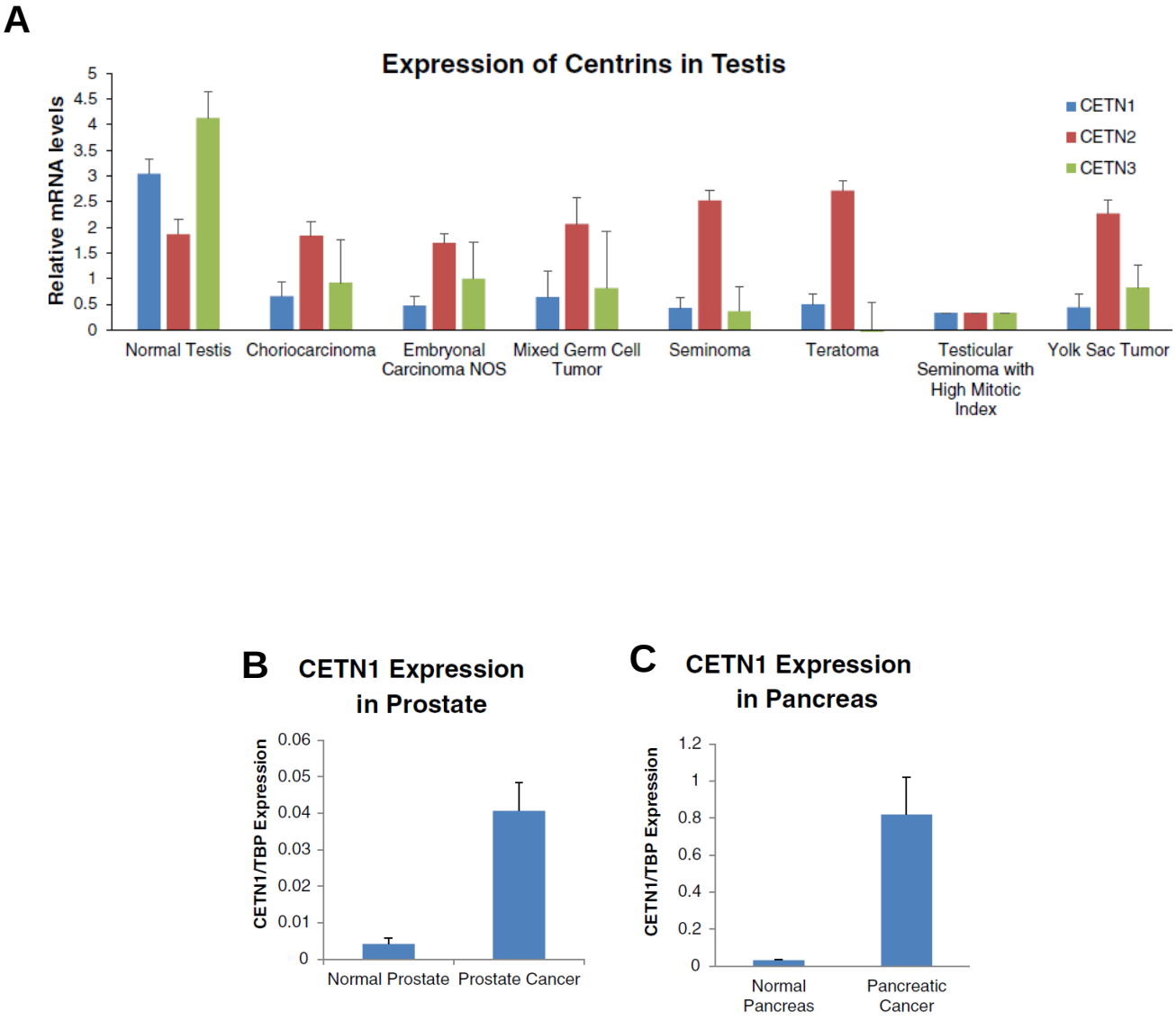

Figure 4. Centrin mRNA and expression levels in testis, prostrate and pancreas

[Adapted from Kim et al, 2013][3] (A) Centrin1/2/3 expression levels differ in normal testis when compared with diseased tissue. (B) and (C) Centrin1 expression in prostrate and pancreatic cancer. Centrin 1 expression shows a 10 fold increase in prostate cancer (B) versus a 25 fold increase in pancreatic cancer(C).

2.3 Centrin targets: HSfi1p

Centrin interacts with several biological targets. One of these targets is *S*fi1, a protein that is co-localized with centrin to the centrioles, the centrosome, basal bodies and the spindle pole bodies (SPB) in yeast. Sfi1 is a protein that ranges from 946 amino acids in yeast to 1242 amino acids in humans and has a largely absent secondary structure. However, in the presence of centrin it adopts a helical contracted structure (Figure 5, Figure 6B). There are twenty-three and seventeen centrin binding sites in human Sfi1 (*Hs* Sfi1) and *Saccharomyces cerevisiae* (*Sc* Sfi1) respectively (Figure 6A). These centrin binding sites form along a series of internal repeats. The centrin-Sfi1 complex forms contractile fibers that are dependent on Ca^{+2} concentrations. These fibers also function to reorient centrioles and alter centrosome structure[40].

Because both centrin and Sfi1 are highly conserved in many organisms, the SPB serve as centrosome analogs that enable gathering of information of their mammalian counterpart. Sfi1p in lower eukaryotes is involved with the SPB half bridge, where SPB duplication is initiated[41] and it has been suggested to mediate interactions necessary for bridge separation[42]. Human Sfi1 *(Hs* Sfi1) is known to function in tandem with centrin[1,43] as a core structural protein in the matrix tethering the two centrioles together and in the assembly of such structures.

During the last decade, a lot of information has come forth about the working of the SPB and its role in yeast cell cycle regulation[44]. However, the involvement of these proteins in the mammalian centrosome and its possible regulatory function is less clear.

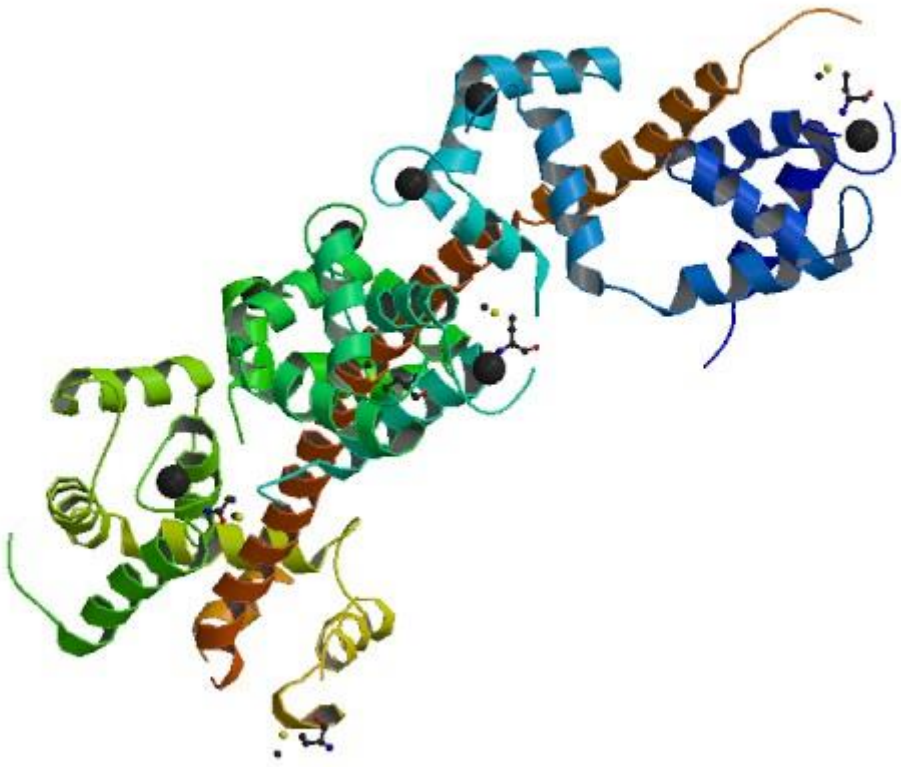

Figure 5. Sfi1p-centrin in budding yeast spindle pole body (PDB Id 2DOQ)

Saccharomyces cerevisiae centrin interacts with Sfi1p via 17 known binding sites, contracting and allowing Sfi1p to form a helical structure[2] (red helical ribbon).

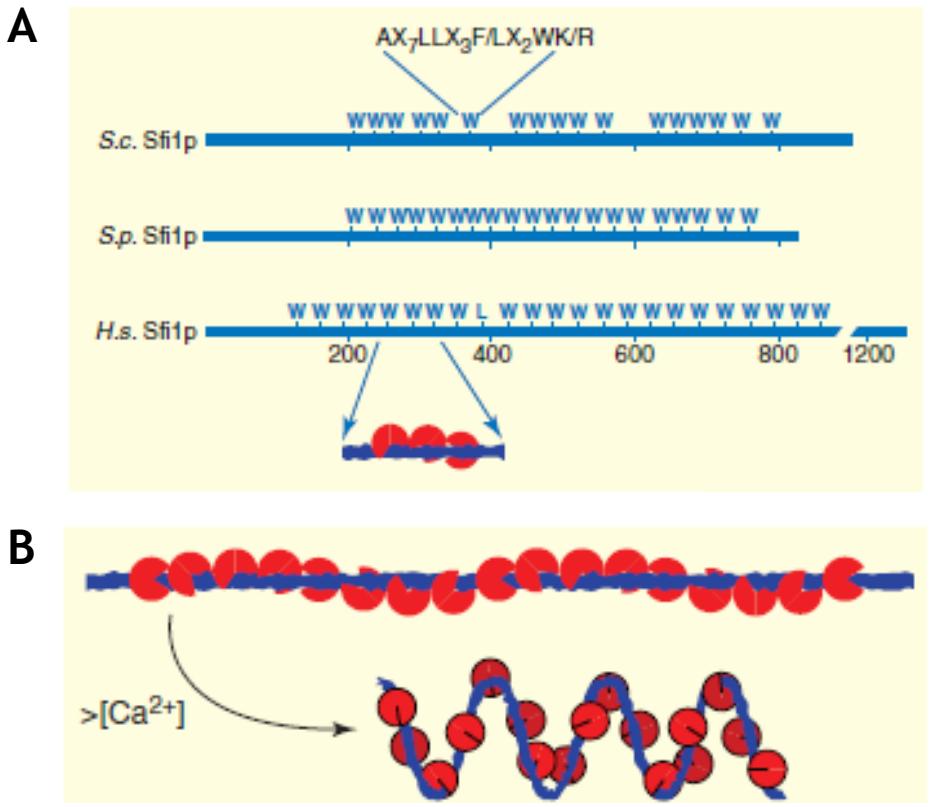

Figure 6. Comparison of the general structure of centrin binding sites and a model for Sfi1p-centrin molecular contraction

[Adapted from Salisbury, 2004][40] The domain organization of Sfi1p orthologs of *Saccharomyces cerevisiae* (*Sc*Sfi1p), *Schizosaccharomyces pombe* (*Sp*Sfi1p), and humans (*Hs_Sfi1*) are depicted above (A**)**. The position of a consensus centrin binding repeat is marked by a W. *Hs_Sfi1* has twenty-three centrin (red in model) binding sites. (B) Centrin molecules attach to the Sfi1p (blue rod) backbone as the concentration of Ca^{+2} ions increases, shortening the overall length of the molecular complex.

2.4 Centrin targets: Human Krr1

A novel biological target for centrin is Krr1. Krr1 is a small subunit (SSU) processome component homolog found in yeast, slime mold, mice, and humans[45]. It is located inside a dark, dense, roughly spherical area of fibers and granules within the nucleus of the cell, called nucleolus[46]. This protein is involved in ribosome biogenesis and RNA processing. It is also required for 40S ribosome biogenesis and is implicated in nucleolar processing of pre-18S ribosomal RNA and ribosome assembly.[47,48]

Human Krr1 has a sequence of 381 amino acids (Figure 7) and a theoretical pI of 9.78, with a large number of charged residues. Krr1 also harbors a KH domain. Mutations in the KH domain of RNA binding proteins have been associated with the fragile X syndrome[49], which includes symptoms such as autism and mental retardation. Krr1 interacts with similar centrin binding targets in *Saccharomyces cervisiae*, such as SUMO2[50] as well as with USP44 and USP49[51]. The interaction between centrin and Krr1 has only recently been confirmed by yeast two-hybrid system (Y2H), (Dr. Walter Chazin personal comunication). Interestingly, information regarding Krr1 is limited and human Krr1 research remains a novel area of study.

```
        10         20         30         40         50         60
MASPSLERPE KGAGKSEFRN QKPKPENQDE SELLTVPDGW KEPAFSKEDN PRGLLEESSF
        70         80         90        100        110        120
ATLFPKYREA YLKECWPLVQ KALNEHHVNA TLDLIEGSMT VCTTKKTFDP YIIIRARDLI
       130        140        150        160        170        180
KLLARSVSFE QAVRILQDDV ACDIIKIGSL VRNKERFVKR RQRLIGPKGS TLKALELLTN
       190        200        210        220        230        240
CYIMVQGNTV SAIGPFSGLK EVRKVALDTM KNIHPIYNIK SLMIKRELAK DSELRSQSWE
       250        260        270        280        290        300
RFLPQFKHKN VNKRKEPKKK TVKKEYTPFP PPQPESQIDK ELASGEYFLK ANQKKRQKME
       310        320        330        340        350        360
AIKAKQAEAI SKRQEERNKA FIPPKEKPIV KPKEASTETK IDVASIKEKV KKAKNKKLGA
       370        380
LTAEEIALKM EADEKKKKKK K
```

Figure 7. Krr1 amino acid sequence

Homo sapiens Krr1 has 381 amino acids in its sequence with a large number of charges residues and a theoretical pI of 9.78, making it a highly soluble protein. Krr1 has a molecular weight of 43.6 kDa and possesses one KH domain containing 53 amino acids from residues 154 – 206.

However, the construction of a search pattern can reveal potential interactions between a known protein and a novel target. A search pattern (Figure 8) was generated via known centrin ligands and sequence alignment tools to use for comparison with the full length small subunit procesome component Krr1. These hits reveal a potential binding site for centrin within the Krr1 sequence.

Measuring interactions between centrins and their target proteins has the potential to better elucidate the mechanisms by which cell division is controlled and as such provide clearer insight on their role in cancer mechanics. A way to determine potential interactions between centrin and its target proteins on a molecular level is the use infrared spectroscopy.

Hits by patterns for [RK]-xxxxxxxx-[LW]: [8 hits on 1 sequence]

24 - 33:	KpenqdeseL
163 - 172:	RligpkgstL
168 - 177:	KgstlkaleL
225 - 234:	KrelakdseL
230 - 239:	KdselrsqsW
280 - 289:	KelasgeyfL
349 - 358:	KvkkaknkkL
352 - 361:	KaknkklgaL

Figure 8. Possible centrin binding sites

These potential binding sites were generated by comparing different known centrin targets and their binding sites (Appendix A).

2.5 Studying Protein-Protein Interactions: FT-IR Spectroscopy

Fourier Transform Infrared Spectroscopy (FT-IR) is a technique used to obtain the infrared spectra of different samples. It works by shining infrared radiation on a sample and seeing which wavelengths of radiation in the infrared region of the spectrum are absorbed by the sample. Each compound has a characteristic set of absorption bands within the Mid infrared region of the spectrum (4000 – 1000 cm^{-1}). These spectra result from transitions between quantized vibrational energy states. In FT-IR spectrometry, all the wavelengths are measured at the same time via the Michelson interferometer. FT-IR spectroscopy provides information about the vibrational modes associated with the backbone of the proteins. It is therefore sensitive to the secondary structure changes within proteins, unlike X-ray crystallography and NMR spectroscopy which provide high resolution information for detailed secondary and tertiary structure. Studies with proteins of known structure have been used to correlate systematically the shape of the amide I band located within the mid IR region (1700-1600 cm^{-1}) to secondary structure content.[52,53] The amide I band results from the C=O stretching vibration of the amide group coupled to the stretching of the C-N bond. In addition, the amide II band is comprised mainly of in plane bending of the N-H bond. These vibrational modes, present as infrared bands between 1600-1700 cm^{-1}, are sensitive to hydrogen bonding therefore causing the bandwidth to increase.

When a protein is dissolved in water the hydrogen attached to the amide nitrogen can readily exchange for hydrogen attached to water molecules. When a polypeptide folds, many of the amide hydrogens become buried in the interior of the protein and no longer come into direct contact with the solvent water. Hydrogen isotope exchange is a

powerful tool for studying the protein folding process.[54] To observe the rate of hydrogen exchange the deuterium isotope of hydrogen (^2H) is used for the solvent water. Because it has twice the mass of ^1H, the exchange results in an appreciable shift in the amide I band (amide I')[55]. It proves a useful technique for measuring interactions between proteins.

Two dimensional correlation (2D-COS) spectroscopy takes advantage of the information provided by FT-IR spectra, to study the formation of relations between events in an experiment, as in the scheme in Figure 9. Studies of putative protein models have been previously done using this technique[56,57]. Centrin analogues in model organisms have also been studied via 2D IR correlation spectroscopy[58], leading to the understanding of molecular events within these highly conserved proteins. Perturbation-correlation two-dimensional spectroscopy has proved advantageous in defining specific characteristics of protein motifs[59] for a particular subject. Recently, this technology has been used to generate a patent on a method for determining aggregation in protein, peptide or peptoid formulations[60,61].

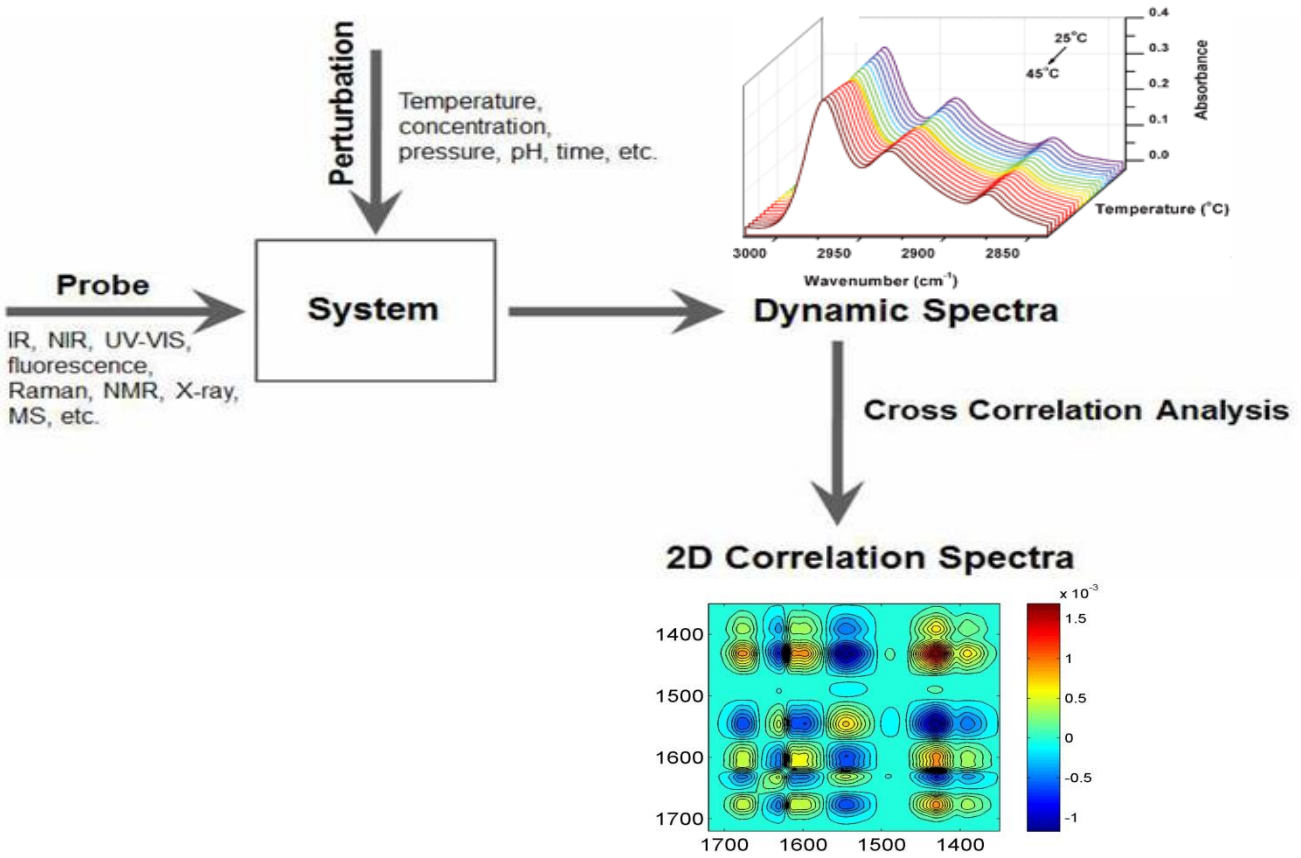

Figure 9. Two-Dimensional Correlation Spectroscopy (2D-COS) Scheme

[Adapted from Noda, 2014][60] In our study a protein sample was subjected to an external perturbation (temperature), the dynamic spectra collected and 2D spectra generated via an algorithm for complex cross correlation.

3 MATERIALS AND METHODS

Reagents and materials used were of the highest quality commercially available. Deionized H_2O with a resistivity of 18 M ohms was also used.

3.1 Biotechnology Aspects

Three expression vectors were used and the following recombinants were generated: pET-100-Krr1, pT7-7-Krr1, pGEX-Krr1 and a final subclone of *Hs* Krr1 with a deleted poly A tail at the 3' end of the sequence termed pT7-7-Krr1NoK. All subclones were sent for cDNA sequencing to Dr. Juan Martínez Cruzado at the Genome Center at the Biology Department. The results obtained corroborated the desired inserts, their correct orientation and reading frame. Each subclone[62] was then transformed into *Escherichia coli* BL21 (λDE3) STAR (Invitrogen, Life Technologies) strain for expression. This particular bacterial strain was chosen because of its ideal use with bacteriophage T7 promoter-based expression systems. The T7 promoter provides a tight expression of the desired recombinant with little to no basal level expression.

Small scale expressions were performed using 15 mL of Terrific Broth II media from MP Biochemicals (Solon, Ohio, USA). To determine expression levels and proper induction SDS-PAGE were done. This validation was a necessary and cost effective step, prior to proceeding with the large scale fermentation process.

3.1.1. Fed-batch Fermentor Expression of Krr1

For the production of large quantities of the desired recombinant protein, overnight cultures were prepared as follows: 200 µL of a bacterial stock of newly transformed

competent *E. coli* BL21 (λDE3) STAR from Invitrogen with the desired recombinant were used to inoculate 250 mL of Terrific Broth containing 50 µg/mL of ampicillin and incubated at 37°C in an orbital shaker at 250 revolutions per minute (rpm) for a period of 14 hours.

Using an autoclaved 4L Biostat A plus bioreactor from Stedim Sartorius located at the Bioprocess Development and Training Center (BDTC) at the Guanajibo Research and Innovation Park, in Mayaguez, the overnight culture was used to inoculate 2L of sterilized Terrific Broth media containing 50 µg/mL of ampicillin for six to seven hours. Hourly aliquotes consisting of 1.00 mL of the on-going fermentation were taken and bacterial growth ascertained by measuring the pellet cell volume (pcv) using a table top refrigerated centrifuge (Eppendorf Centrifuge 5417R). Once the initial bacterial density measured had duplicated, indicating a change toward the logarithmic growth phase had been achieved, the culture was then induced for the production of the desired recombinant protein by the addition of isopropyl-β-D-1-thiogalactopyranoside (IPTG). The running parameters for the bioreactor were as follows: set at constant temperature of 37°C for optimal growth, acid-base adjustments (using HCl as the acid and NaOH as the base) to maintain a constant pH = 7.00, and agitation set at 300 rpm, along with a constant purge of air and oxygen to ensure aerobic conditions. Once the bacterial cell culture reached the stationary phase, cells were harvested by centrifuging the entire culture for 15 minutes at 9615 x g and 4^{o}C with a JA-14 rotor on a Beckman J2-MC centrifuge. The pellets obtained were stored at a temperature of -80° C for future isolation and purification.

3.1.2. Isolation of recombinant Krr1

Before the beginning of the purification process, the pellet was thawed to perform the lysis and clarification procedure. To the pellet, we added four times its weight the amount of lysis buffer containing 50 mM Tris, 0.5 mM NaCl, 0.1% IGEPAL and 0.04% NaN_3 at a pH of 7.4) and an EDTA-free protease inhibitor cocktail capsule composed of: 2.0 mg/ml aprotinin, 0.5 mg/ml leupeptin, and 1.0 mg/ml pepstatin A. This solution was subjected to a sonicator probe for cycles consisting of one minute sonication and 30 second rest periods on ice. The cycles were repeated until the solution viscocity could no longer be appreciated. Afterwards, the sample was centrifuged for 15 minutes at 9615 xg using a Beckman J2-MC centrifuge. Following this initial centrifugal step, the sample was submitted to an ultracentrifugational step at 70,588 xg for 30 minutes and 4°C using a TI-70 rotor and a Beckman L-80 ultracentrifuge. This centrifuged sample was then clarified by using a 0.1 µm hollow cartridge from GE Healthcare. This process of filtration of the lysate decreases the viscosity of the sample. Only then were the buffer conditions of the recombinant protein sample changed to the loading buffer with low salt conditions by centrifugation using a 20 kD filter from Amicon and a tabletop refrigerated centrifuge Eppendorf model 5810 R.

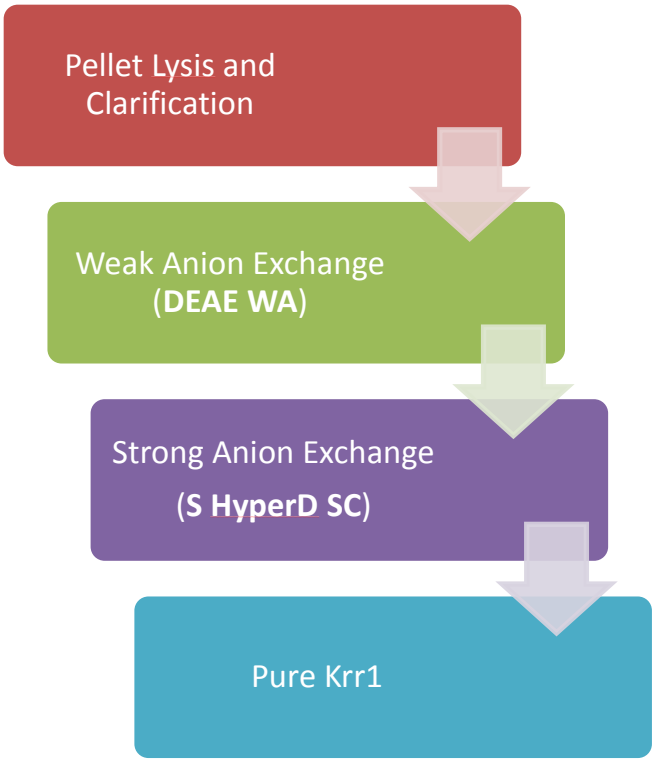

Figure 10. Overview of the Krr1 Purification Process

Each process culminated in an SDS-PAGE analysis of the results before proceeding.

3.1.3. Krr1 purification

The Krr1 sample was subjected to two chromatographic steps: first, an anion exchange chromatography and, second, a strong cation exchange chromatography (Figure 10). We tested this purification protocol using a small scale column with a weak anion exchanger like Acrosep™ DEAE Ceramic HyperD F 1.00 mL pre-packed column, which in turn was carried out according to the reference[31]. The corresponding loading buffer was HQ Strong Anion Exchange (Eluant A) 20mM Tris, 1.0 mM $CaCl_2$, 0.04% NaN_3 and a pH of 7.4. The elution buffers were as follows, (Eluant B) 0.0-0.8M NaCl Gradient, 20mM Tris, 1.0mM $CaCl_2$, 0.04% NaN_3, 0.8 NaCl and a pH of 7.4, HQ Strong Anion Exchange (Eluant C) 40mM Tris, pH 7.4, 0.04% NaN_3, 1.0 M NaCl. The cation exchange chromatography was performed using a strong cation exchanger such as Acrosep™ S Ceramic HyperD F 1.00 mL pre-packed column according to the manual specifications[63]. Both the anion exchange and the cation exchange columns involved a step-wise salt gradient.

3.1.4. Biochemical characterization of recombinant Krr1

Biochemical characterization of the recombinant proteins was performed after they had been successfully purified and a purification protocol established for novel proteins. Pre-cast gradient 4-20 % Bis-Tris SDS-PAGE (sodium dodecyl sulfate polyacrylamide gel electrophoresis) gels from BioRad were used after each bioreactor run to ensure

overexpression of the desired recombinant protein. SDS-PAGE was also performed after each purification step to confirm fractions containing the recombinant protein of interest. Partial amino acid sequencing of the N-terminus was performed to identify the recombinant protein after being subjected to the purification steps.

3.2 FT-IR

3.2.1 Sample preparation

All samples for FT-IR spectroscopy were prepared in the same manner following our established protocol[19,20]. The concentration of purified centrin 1 was determined using UV spectrophotometry at 280 nm, and buffer exchanged to the running buffer conditions (50 mM HEPES, 300 mM NaCl, 4 mM $CaCl_2$ and 4 mM $CaCl_2$ at pH 7.4). The *Hs* centrin 1-*Hs* $Sfi1_{p21}$ complex (1:1 molar ratio) was lyophilized and subjected to repeated re-solubilization with deuterium oxide (D_2O) to generate a fully H→D exchanged complex.

3.2.2 $^{15}N_2$-Arg_{16}*Hs_Sfi1*p_{21} Synthesis

Li and Kilmartin have proposed a salt bridge interaction between Cdc31 E_{97} and scSfi1p R_{256}. We hypothesize the same interaction exists between *Hs* centrin 1 and the arginine residue (R_{16}) of the Sfi1p fragment. The existence of this salt bridge was investigated by synthesizing the Sfi1p fragment 21 incorporating a ^{15}N-labeled arginine via a collaboration with Dr. Robert Ríos group. FT-IR spectroscopy was then used to study the salt bridge interaction of the ^{15}N-labeled arginine (R_{16}) of the Sfi1p fragment 21 with *Hs* centrin 1.

The synthesis of ^{15}N-labeled arginine is depicted in Figure 11. The method used for the synthesis of amino acids was described by Murray *et.al*. and Lipton *et.al*. The synthesis was initiated with ^{15}N-labelled guanidine, commercially available Two of the nitrogens were selectively protected as benzyl carbamates by using benzyl chloroformate and aqueous sodium hydroxide in H_2O/THF. Functionalization of the remaining nitrogen as a triflate was accomplished by deprotonation with sodium hydride followed by quenching of the anion with triflic anhydride. Finally, the ^{15}N-labeled arginine 3 was acquired from addition-elimination reaction of Fmoc-Orn-OMe to 2 followed by the saponification of the methyl ester using LiOH in a 1:1 mixture of THF/H_2O. Fmoc provides the advantage of being cleaved under very mild basic conditions, yet remain stable under acidic conditions. This allows mild acid labile protecting groups that are stable under basic conditions, such as Pbf, to be used on the side-chains of L-Arginine residue of the target peptide. This amino acid (AA) was perfectly suitable for the automation of solid phase peptide synthesis (SPPS) of the proposed Sfi1p fragment.

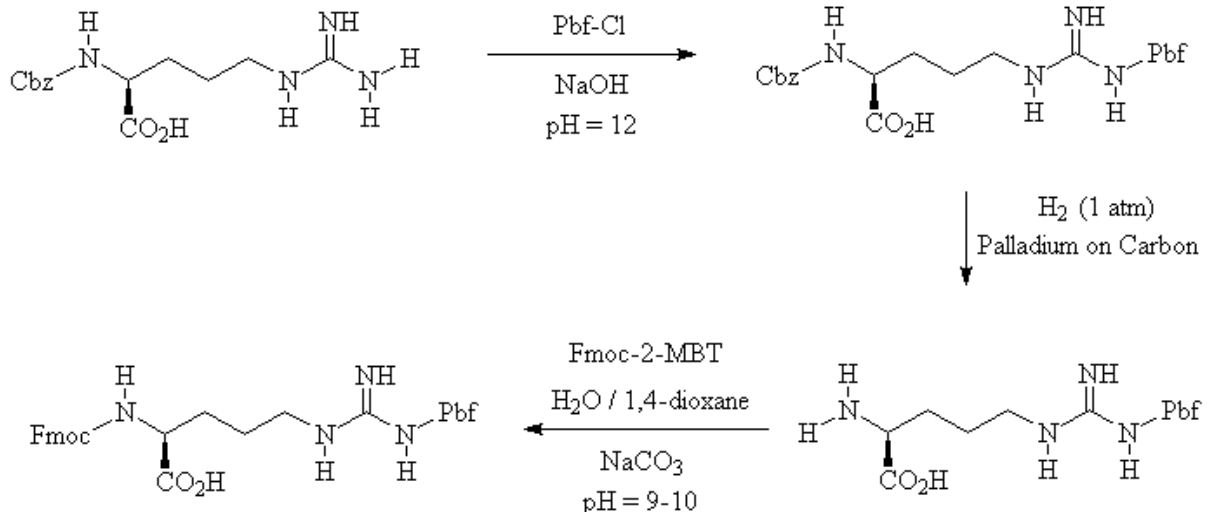

Figure 11. Schematic Synthesis of ^{15}N labeled arginine

The above figure represents the synthesis of selectively labeled, orthogonally protected Fmoc-L-Arginine-guanidino ^{15}N(Pbf)-OH suitable for solid phase synthesis. The target compound was prepared in four steps from the commercially available precursor L-Arginine-guanidino^{15}N.

The existence of the salt bridge on the arginine residue, if confirmed, needs special consideration when planning the synthesis of the inhibitors. We began by studying the structure-activity relationship on the 33 amino acid sequence of *Hs*_Sfi1p fragment 21 shown in Figure 12.

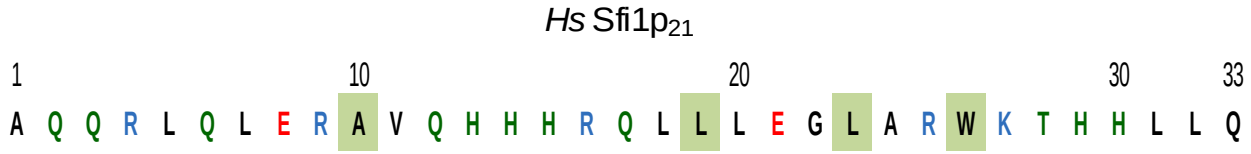

Figure 12. *Hs_Sfi1*p$_{21}$ centrin binding site chosen for the exploration of *Hs*cen-*Hs_Sfi1*p interaction.

*Hs_Sfi1*p$_{21}$ centrin binding site chosen for the exploration of *Hs*cen-*Hs_Sfi1*p interaction. Key interactions that will be explored are Arg 16 to examine the effect of the salt-bridge interaction.

3.2.3 Running Conditions

Previously D_2O exchanged samples and the reference buffer were re-suspended in 60 µL of D_2O and placed in the middle of calcium fluoride 49 mm x 4 mm cells. Both the reference and sample cells were then sealed with a mixture of chloroform and mineral oil. The cells were positioned inside a temperature and humidity controlled chamber within the FT-IR equipment (Jasco FTIR-6200 mid IR range, equipped with a narrowband MCT detector). The gasket containing the cells was surrounded by a water bath (NESLAB RTE 740, Thermo Fischer) to change the temperature of the samples during the experimental run. Typically, 512 scans were co-added, apodized with a triangular function and Fourier transformed to provide a resolution of 4 cm^{-1} with the data encoded every 2 cm^{-1}.

3.2.4 2D IR Correlation Spectroscopy

The spectral data for the FT-IR spectral analysis was baseline corrected and thermal dependence plots were generated using Origin version 7 from OriginLab Corp. The spectra were collected at regular intervals during the thermal perturbation. The spectral overlay, peak pick routines, and 2D IR correlation analysis were performed using a Kinetics program for MATLAB (MathWorks, Natick, MA) generously provided by E. Goormaghtigh (Free University of Brussels, Brussels, Belgium).

4. RESULTS AND DISCUSSION

4.1 Bacterial transformations

Bacterial transformation was confirmed by evaluating successful colony formation. An example of the obtained results can be seen in Figure 13. Few positive colonies were present in both plates. These results, however, demonstrate the effective generation of a modified recombinant protein Krr1NoK expressing clone.

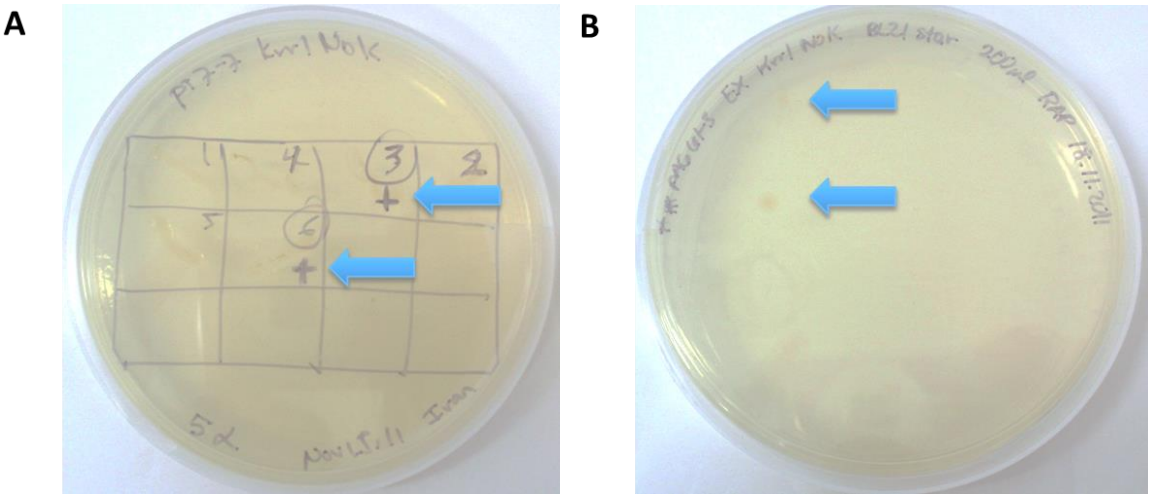

Figure 13. Example of Successfully Transformed Clones for pT7-7 Krr1NoK

The arrows point to two different colonies indicating successful transformation of bacterial cells. A small sample was in turn used for small scale protein expression.

4.2 Bacterial Expression of human Krr1

Multiple batches of bacterial expression for the recombinant protein Krr1 were performed. *E. coli* BL21-STAR (DE3) transformed competent cells were used for three different constructs pGEX-Krr1, pT7-7 Krr1 and pT7-7Krr1NoK (Figure 14) and grown in Terrific Broth media. The plotted growth curves from Figure 14 show good growth as seen by the typical sigmoidal curve in which all reached similar stationary phase at a pcv of 10 μL, with clones pGEX-Krr1 and pT7-7 Krr1 growing at a similar rate. Clone pT7-7Krr1NoK grew at a slower rate. Induction with IPTG was done when the sampled pellet cell volume doubled. Bacterial growth was stopped after the culture had reached constant pellet cell volume, typically after 6-8 hours as shown in Figure 14. One mL aliquots were taken from the culture every hour to evaluate the bacterial fermentor of the specific Krr1 recombinant expression level, by SDS-PAGE shown in Figure 15.

After protein expression was confirmed, samples from the clarification process were taken and ran through an SDS-PAGE (Figure 17b).

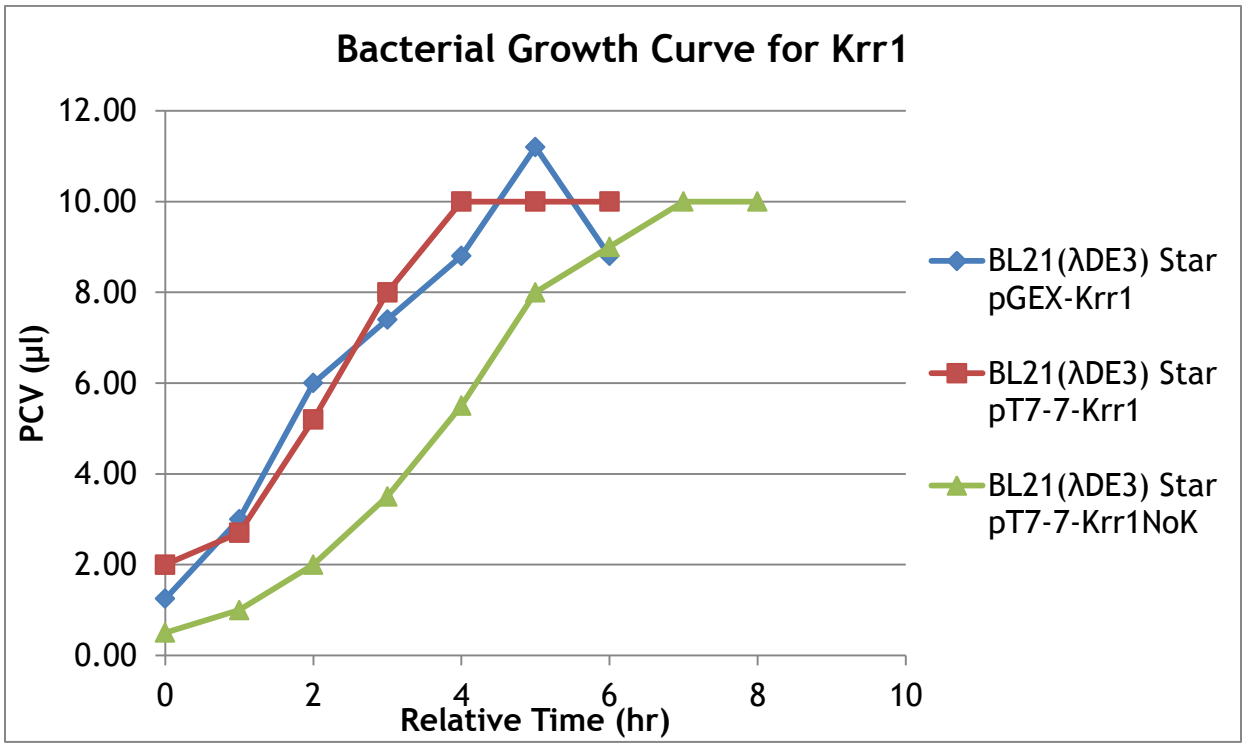

Figure 14. Superimposed growth curves for recombinant protein Krr1.

Three constructs were made and examined for cell growth. These superimposed growth curves show a similar growth pattern between all clones.

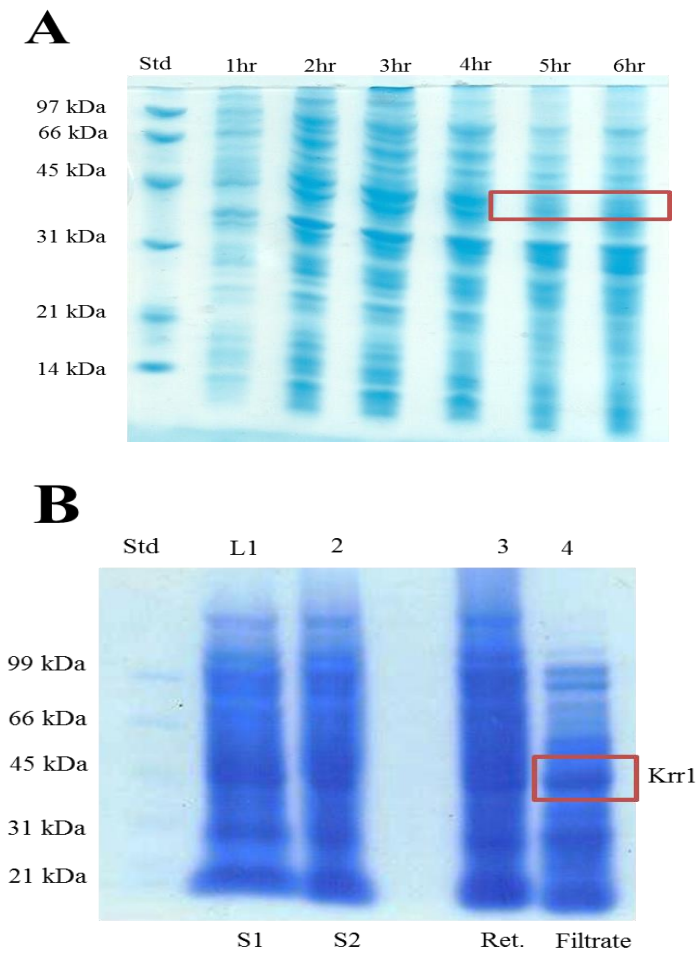

Figure 15. SDS-PAGE results for expression.

(A) *E. coli* BL21 (λDE3) STAR pT7-7 Krr1 construct after each hour of growth and (B) subsequent lysis and clarification of the sample. S_1 and S_2 are the supernatant samples taken after each centrifugation step.

4.3 Purification of Krr1

4.3.1 Anion Exchange Chromatography

Clarified samples of Krr1 were buffer exchanged to loading buffer A (20mM Tris, 1.0 mM $CaCl_2$, 0.04% NaN_3 and a pH of 7.4) to remove all salts previous to loading the column. A step-wise salt concentration increase with elution buffer B (0.0-0.8 M NaCl Gradient, 20mM Tris, 1.0mM $CaCl_2$, 0.04% NaN_3, 0.8 NaCl and a pH of 7.4) was used to remove contaminant proteins (Figure 16). The steps in the elution consisted to 0% to 100% buffer B with a final passing of a high salt elution buffer C (40mM Tris, pH 7.4, 0.04% NaN_3, 1.0 M NaCl). Two large defining peaks were observed, one in the void volume (0% buffer B) labeled Peak A, and one at 80% buffer B, labeled Peak B. Because Krr1 has a high isoelectric point (pKa of 9.78), at the current pH of the solution it has may positively charged residues. These positive charges would not enable the protein to interact with the matrix of an anion exchange chromatography column; therefore we believe that it elutes in the void volume, as the labeled Peak A marked in Figure 16. The remaining peak at 80% salt concentration is attributed to the presence of bacterial contaminant proteins. This initial step was of great importance in the preliminary removal of contaminants.

Samples were collected from each observed peak, and ran through an SDS-PAGE to evaluate protein presence (Figure 17).

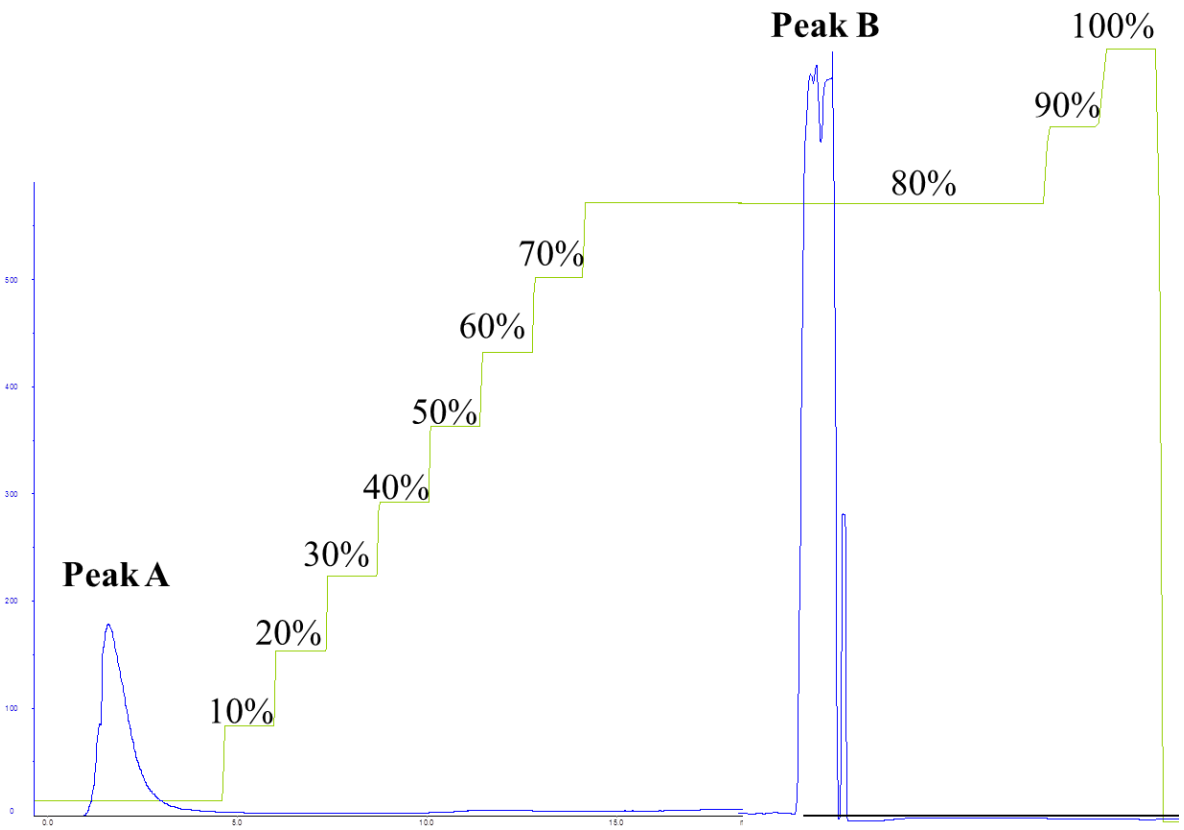

Figure 16 . Weak Anion Exchange Chromatogram for Krr1.

A separation of components can be seen via a step-wise salt gradient ranging from 0%-100% of a saline buffer. Two peaks were observed, peak A during the void volume step and a second peak B corresponding to a lower pKa value.

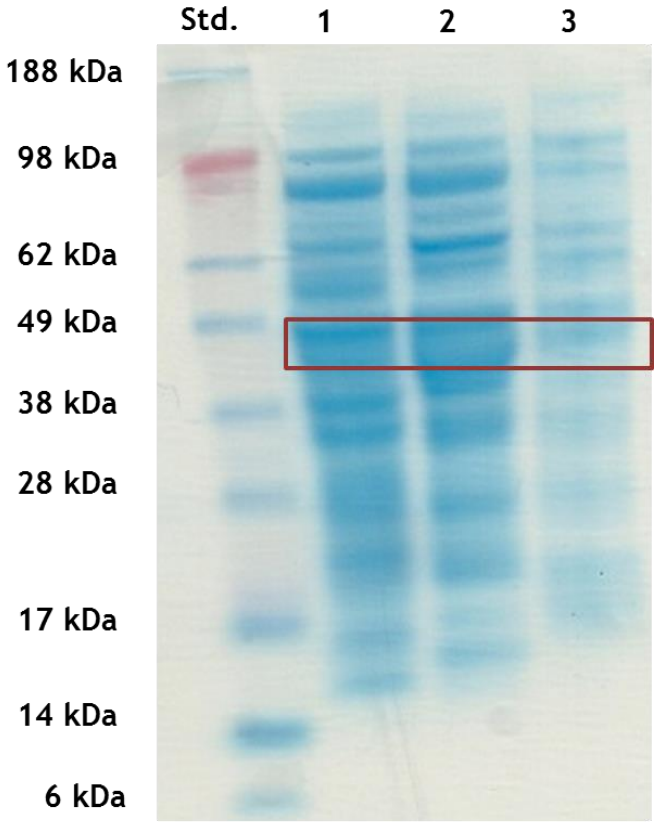

Figure 17. SDS-PAGE analysis of DEAE Anion Exchange Column samples.

Lanes 1-3 represent the void volume from different runs on the DEAE anion exchange column. The presence of Krr1 can be seen between molecular weight markers 49 kDa and 38 kDa.

4.3.2 Cation Exchange Chromatography

Pooled samples from the anion exchange void volume were changed to a buffer without sodium chloride and passed through a strong cation exchange column (S HyperD column) for further purification. For this process, a step-wise buffer gradient was used. During the run, buffer conditions were changed by increasing the sodium chloride concentration (increasing Buffer B) in a gradient and leaving it in that step for 10 column volumes. The positive residues in *Hs*Krr1 allow the protein to interact with the negatively charged residues of a strong cation exchange column matrix.

Figure 18 shows an example of a typical chromatogram. A small peak was observed in the void volume as well as a large peak at 10% of buffer B (Figure 18A). This last peak starts at the transition from 0-10% buffer B and ends during the 10% B step. Two distinct peaks were seen at the 50% B step (Figure 18B), conclusive with the expected *Hs*Krr1 elution. These peaks were collected and ran through an SDS-PAGE (Figure 19). The bands shown in the gel at ~45 kDa confirm the presence of *Hs*Krr1 which has a molecular weight of 43.6 kDa. However, the bands seen were faint, indicating a low concentration of protein even after concentrating the samples.

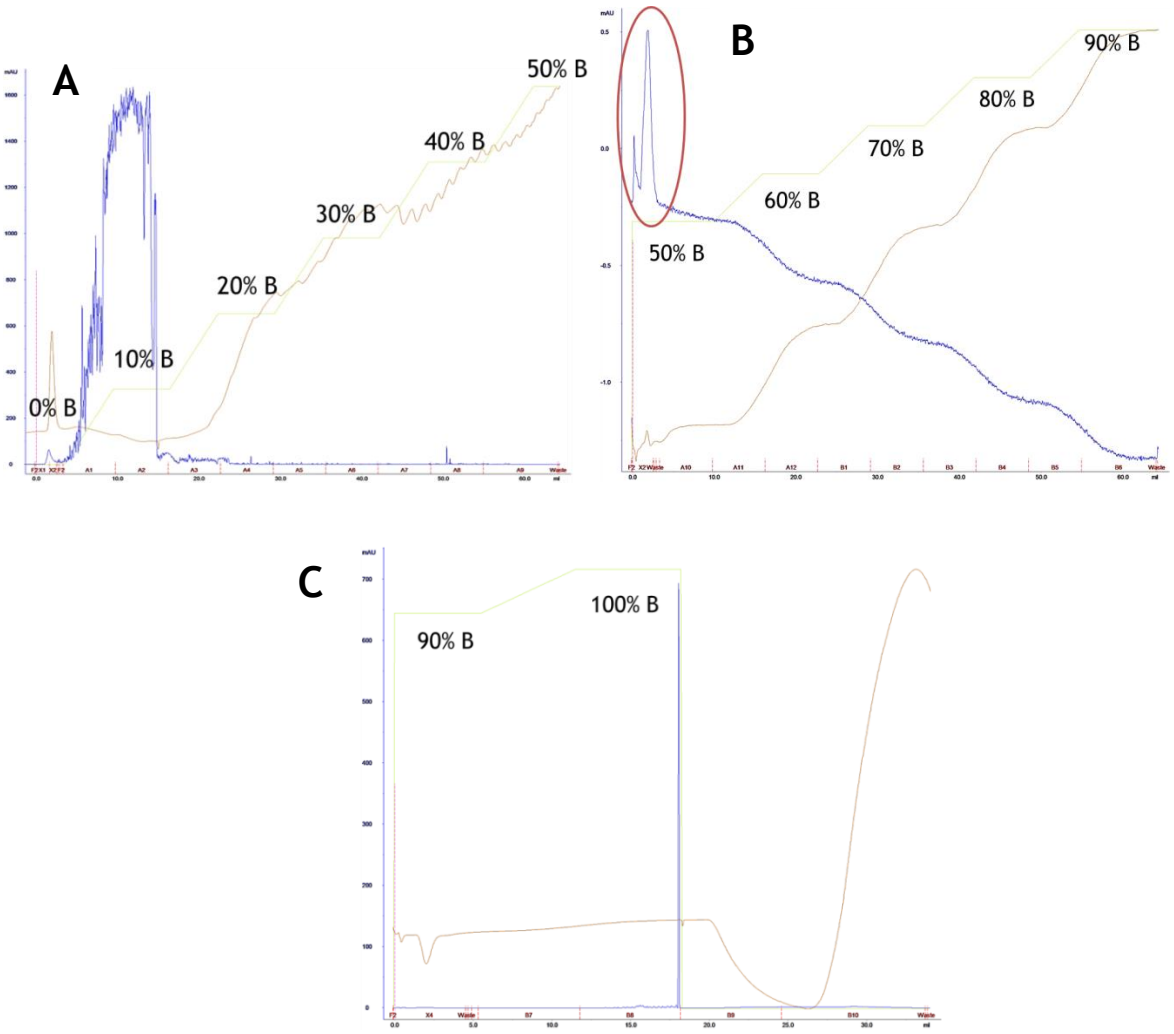

Figure 18. Example of a typical Cation Exchange Chromatogram.

(A) Step-wise gradient results from 0% to 50% buffer B wherein a large peak is observed in the void volume. (B) Step-wise gradient results from 50% to 90% buffer B that show the expected peak corresponding to Krr1 at 50% buffer B, and (C) Step-wise gradient from 90 % to 100 % buffer B.

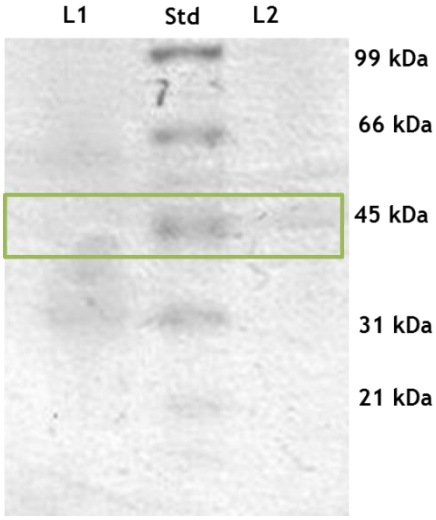

Figure 19. SDS-PAGE of Pooled Samples from Cation Exchange Chromatography.

Lanes 1 and 2 represent the pooled fractions of the peaks observed at 50 % buffer B from different runs. Highlighted is the expected molecular weight of HsKrr1. A very faint band is observed due to the low concentration of protein present.

4.3.3 Cation Exchange Membrane

Another method that was tried after collecting fractions during the anion chromatography step was the use of a cation exchange membrane (Mustang S 0.8 µm cation exchange membrane) in place of and before a cation exchange column. A representative chromatogram of that process is shown in Figure 20. The concentration of salt was increased by steps consisting of 20 %, 40 %, 60 %, 80 % and 100% buffer B. A large peak was observed in the void volume at 0 % buffer B indicating the removal of contaminant proteins. Another large peak was observed at 60 % buffer B and a smaller peak was also seen during the 80 % buffer B step. Fractions from 60 % buffer B and 80 % buffer B were collected and analyzed by SDS-PAGE. However, the bands present in the gel were very faint indicating low recovery from this chromatography step and also a low overall yield.

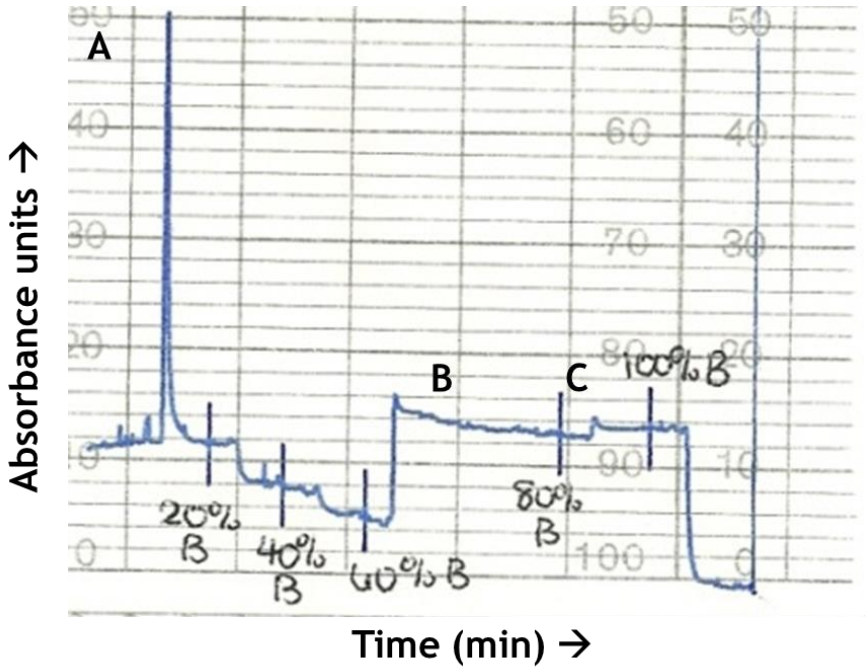

Figure 20. Chromatogram of Cation Exchange Membrane Mustang S 0.8 µm.

A distinctive representation of a chromatogram observed during the membrane step. The concentration of salt was increased by steps consisting of 20 %, 40 %, 60 %, 80 % and 100% buffer B. Each line along with the buffer concentration indicates the start of a particular step. (A) A large peak is observed in the void volume at 0 % buffer B indicating the removal of contaminant proteins. (B) A large peak is observed at 60 % buffer B. (C) A small peak can be observed during the 80 % buffer B step.

4.3.4 Experion Microchip Electrophoresis

Common SDS-PAGE systems require a minimum protein concentration of 3–5 µg/µl to be able to visualize a well-defined band. The low protein yield observed during the final chromatography stages could not satisfy that requirement. Instead a microchip PAGE analysis, which allows the detection of protein presence from low concentrations (ng/µl), was used. Samples corresponding to different chromatography steps were buffer exchanged, concentrated and ran through the microchip PAGE (Figure 21 and Figure 22). A band around the expected molecular weight of *Hs*Krr1 is seen in lanes 3 and 4 of Figure 21. These lanes correspond to fraction obtained from the cation exchange chromatography column (lane 3), the void volume observed during the cation exchange assay (lane 4) and the fraction collected at 80 % buffer B during the cation exchange chromatography assay (lane 5). Figure 22 shows a closer look at the data obtained from the microchip PAGE, by comparing the resolution of protein separation from each lane in which a band associated with *Hs*Krr1 was observed. Here the results showed good separation of proteins with similar molecular weights as well as the overall composition of the analyzed sample. When comparing the sample plots with the molecular weight standard plot (Figure 22A) the level of purity can be estimated. Peaks observed at 0 % buffer B in the Mustang S samples (Figure 22C) indicate the presence of contaminant proteins along with our desired protein. Nevertheless, the plots for S HyperD cation exchange column (Figure 22B) and for Mustang S cation exchange membrane (Figure 22D) showed a distinct peak at the expected molecular weight for *Hs*Krr1 (43.6 kDa). These results demonstrate the efficacy of the purification methods used in this study.

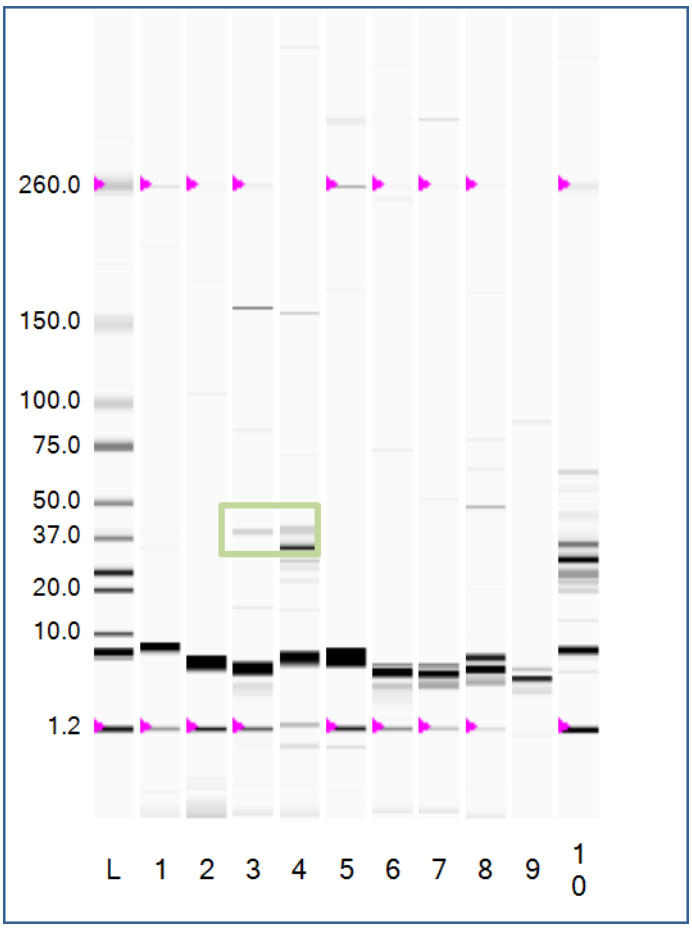

Figure 21. Experion Microchip Electrophoresis Results.

The lane marked L corresponds to the molecular weight standards. The highlighted bands on lanes 3 and 4 correspond to the presence of Krr1 in those samples.

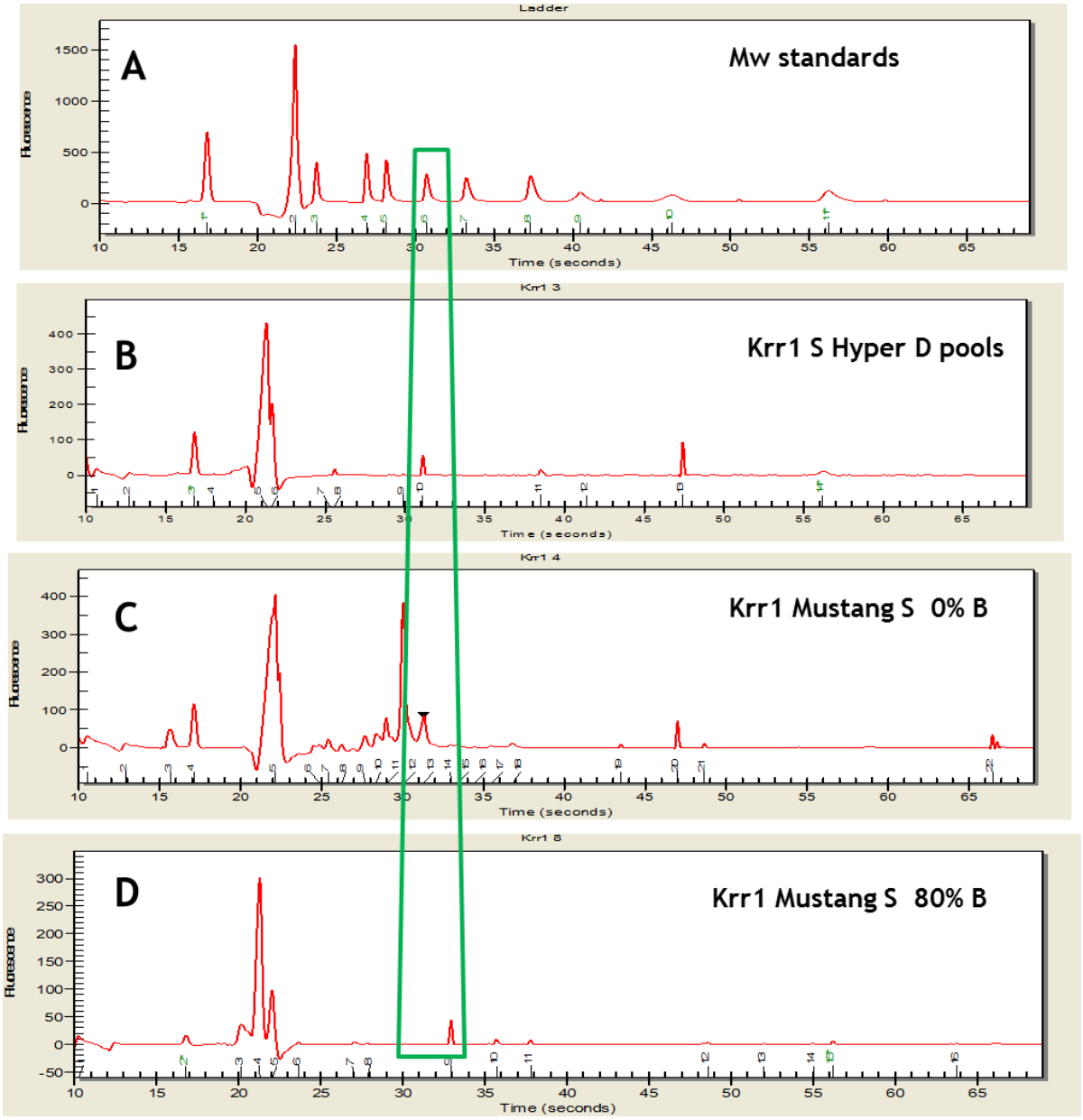

Figure 22. Comparative resolution results from Experion Microchip Electrophoresis from different purifications

(A) Molecular weight standards are compared with (B) pooled samples from strong cation exchange column S Hyper D, (C) the fraction collected from the void volume of the cation exchange membrane, and (D) the fraction collected from the 80% buffer B peak observed in the cation exchange membrane. Highlighted is the peak corresponding to the molecular weight of Krr1 (43.6 kDa).

4.4 The *Hs*_cen1-$^{15}N_2$-Arg_{16}*Hs*_*Sfi1*p_{21} complex

In 2006, Li and Kilmartin[2] proposed a salt bridge interaction between *Saccharomyces cerevisiae* centrin Cdc31 and scSfi1p via the close proximity of the glutamate residue of Cdc31 and an arginine residue of scSfi1p. We hypothesize the same interaction exists between glutamate residues of *Hs*_centrin1 and the arginine residue (R_{16}) of the *Hs*_Sfi1p21 fragment. This interaction was studied via the use of fourier transform mid range infrared spectroscopy and two dimensional correlation spectroscopy using the *Hs*_*Sfi1*p21 fragment labeled with ^{15}N. This isotope labeling accounts for a slight shift in the Amide II' region.

Previous research on proteins with well-known secondary structure has provided information on the shape of the amide I' band (1700-1600 cm^{-1}) and the amide II' band (1575-1480 cm^{-1}). The amide I' peaks correspond to secondary structure components such as α-helix (~1641 cm^{-1}, ~1653 cm^{-1}), β-turns, random coil (1645 cm^{-1}) and certain amino acid side chain contributions such as glutamate and aspartate. For the purpose of this study, the amide II' peak focuses on the contribution of arginine as an amino acid side chain residue. Contributions for the different structure components can be seen by observing the peaks in the overlay and corresponding synchronous and asynchronous 2D plots (Figure 23). A closer look at the Amide I' maximum peak position in relation to temperature (Figure 24) reveals a sigmoidal shape as the contribution shifts from structured to unstructured (random coil). Nevertheless a constant peak absorbance at ~1643.8 cm^{-1} that begins at 40°C and increases after 50°C is indicative of complex formation and dissociation, respectively.

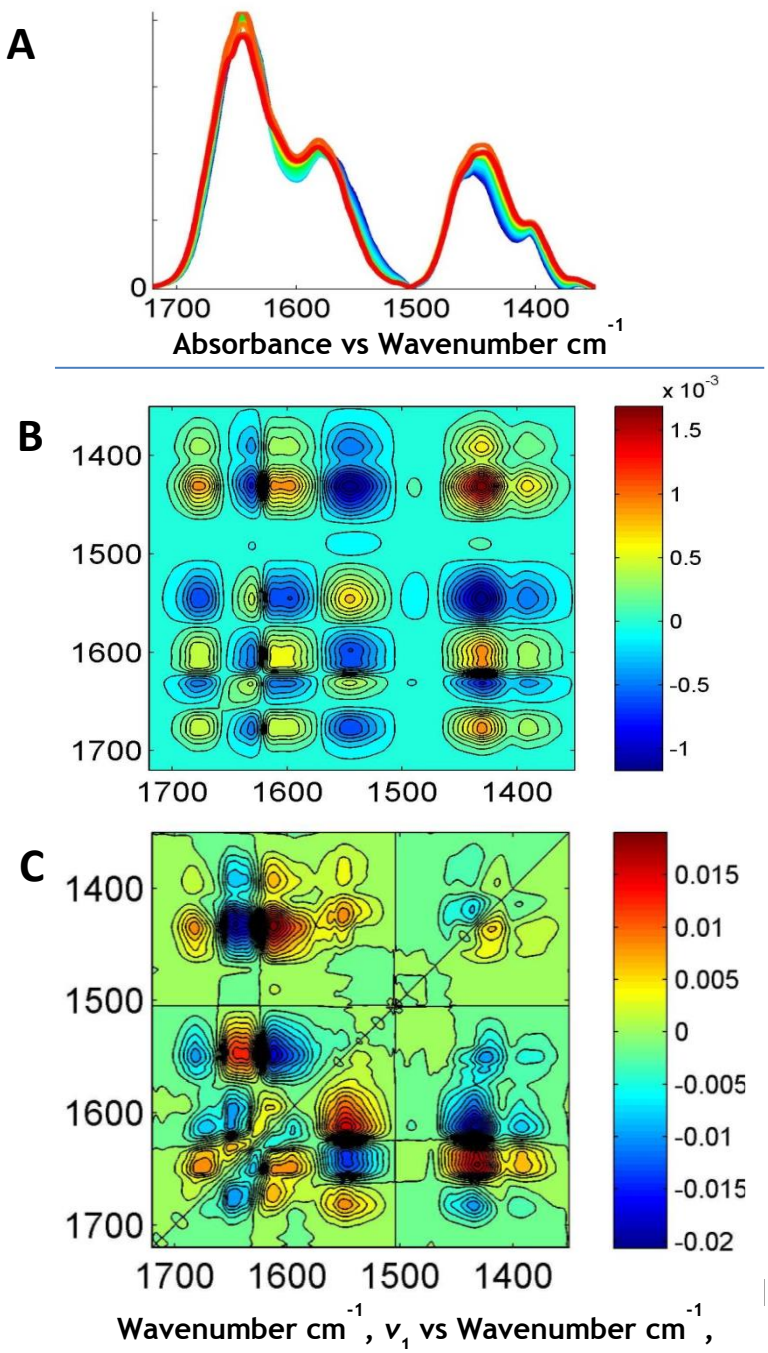

Figure 23. Overlay and 2D Plot of the *Hs*_cen1-$^{15}N_2$-Arg$_{16}$*Hs_Sfi1*p$_{21}$ complex

(A) Full spectra overlay of the amide I' and amide II' regions for the labeled *Hs*_cen1-*Hs_Sfi1*p$_{21}$ complex. (B) and (C) represent the 2D correlation plots. The intensity of the synchronous plot (B) represents simultaneous or coincidental changes of two separate spectral intensity variations. The intensity of the asynchronous plot (C) represents sequential or successive, but not coincidental, changes of spectral intensities measured separately.

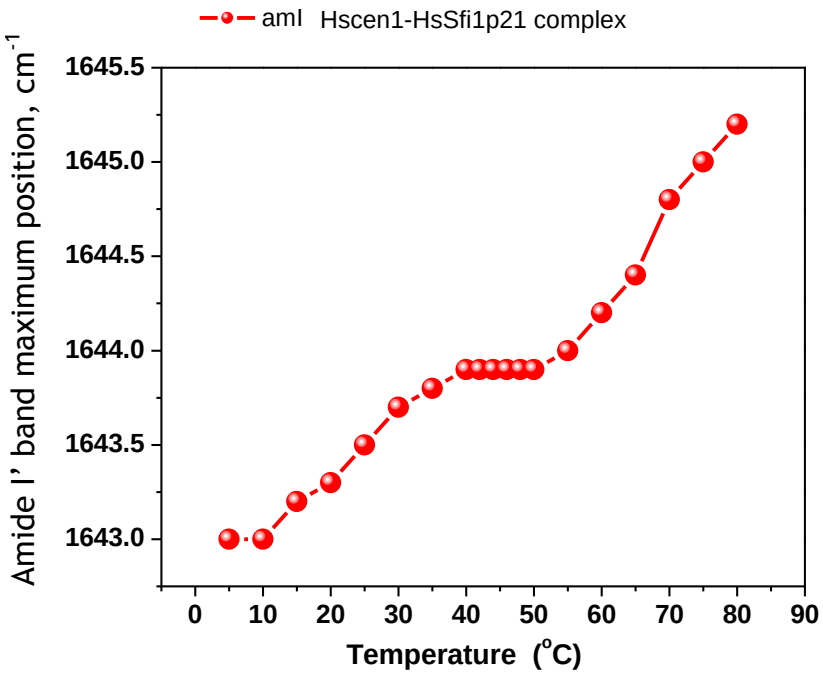

Figure 24. Amide I' maximum peak over temperature for the *Hs*_cen1-$^{15}N_2$-Arg_{16}*Hs_Sfi1*p_{21} complex

The above figure describes the temperature dependence plot for the *Hs*_cen1-$^{15}N_2$-Arg_{16}*Hs_Sfi1*p_{21} complex as observed with the maximum amide I' peak position. A constant peak position in the temperature range of 40-50°C indicates the stable formation of the complex. To better analyze the peak contributions, the subsequent 2D plots were dividing in the stages, before (5-40°C), during (40-50°C) and after complex formation (40-80°C).

To better elucidate the interaction events, the IR spectra and 2D IR plots were separated by temperature ranges as presented in Figure 25-27 . These temperature ranges represent the period before the interaction Figure 25 at 5-40°C temperature range, during complex formation Figure 26 at 40-50°C temperature range and finally the dissociation of said complex Figure 27 at 50-80°C temperature range.

A closer look at the changes occurring in the position of the amide I', side chain interactions and amide II' peak contributions as the temperature increased is depicted in Figure 28. Figure 28 A to C represent the maximum amide I' peak contribution through the steps previous to, during and after the complex formation. The peak contribution of side chain interactions shifts as the temperature increases Figure 28D, while as the temperature increases the peak contribution of the amide II' band shifts to lower wavenumbers Figure 28E. Lastly, a shift in wave number is attributed to part of the contribution of the labeled peptide Figure 28F.

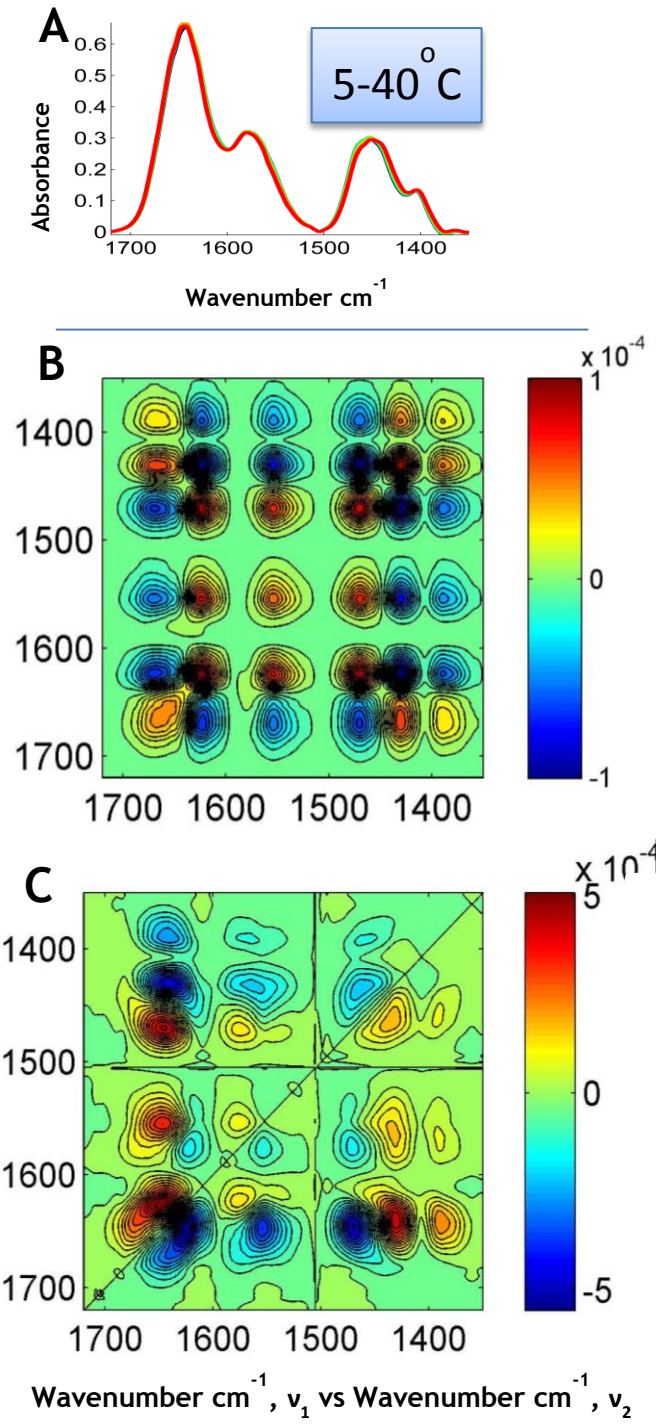

Figure 25. Pre-complex formation for *Hs*_cen1-$^{15}N_2$-Arg$_{16}$*Hs*_*Sfi1*p$_{21}$ from 5-40°C

Part I of the step analysis for the labeled *Hs*_cen1-$^{15}N_2$-Arg$_{16}$*Hs*_*Sfi1*p$_{21}$ Complex. To better elucidate the interaction events, the 2D IR plots were separated into three temperature ranges. The first temperature range is depicted above. (A) Spectral overlay, (B) synchronous plot, (C) asynchronous plot.

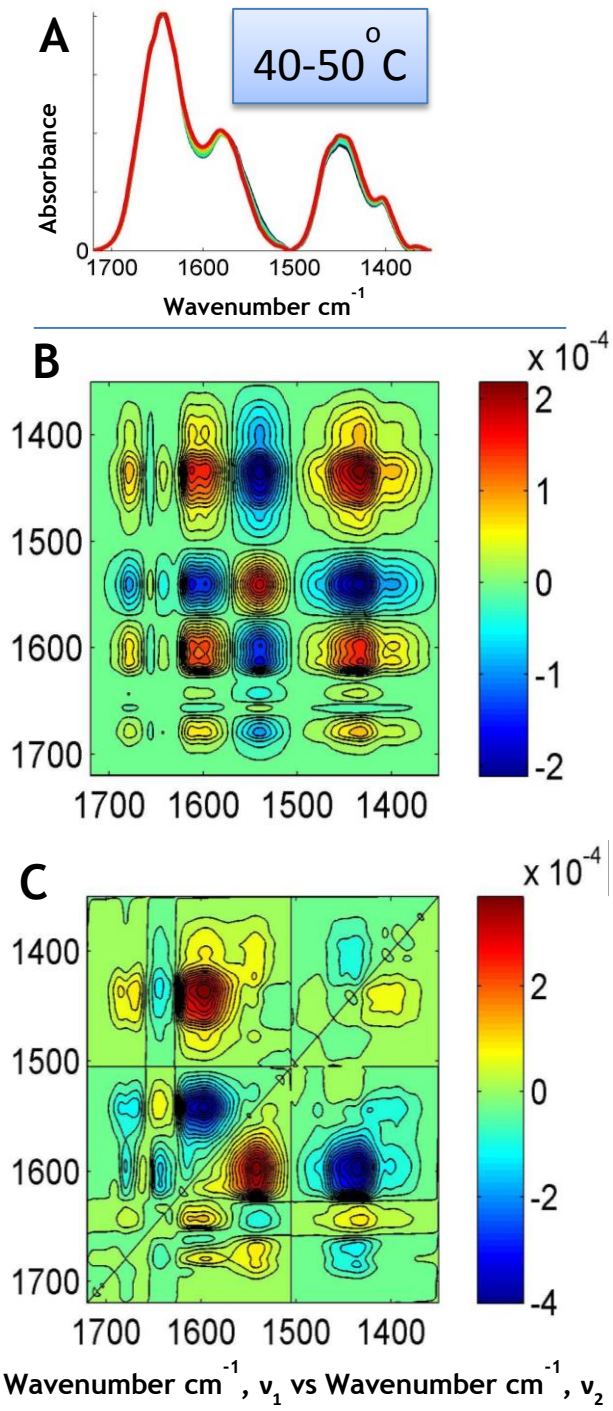

Figure 26. Complex formation for *Hs* cen1-$^{15}N_2$-Arg_{16}*Hs Sfi1*p_{21} from 40-50°C

Part II of the step analysis for the labeled *Hs*_cen1-$^{15}N_2$-Arg_{16}*Hs_Sfi1*p_{21} Complex. The second temperature range is depicted above. (A) Spectral overlay, (B) synchronous plot, (C) asynchronous plot.

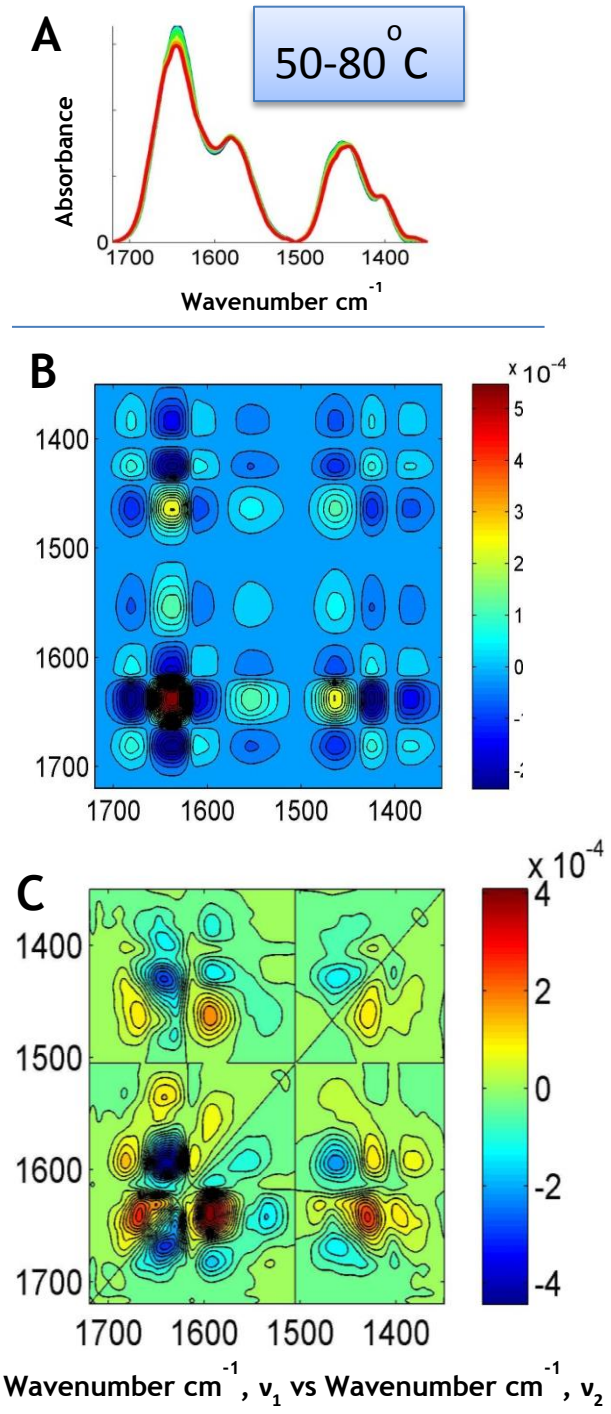

Figure 27. Post-Complex formation for *Hs*_cen1-$^{15}N_2$-Arg_{16}*Hs_Sfi1*p_{21} from 50-80°C

Part III of the step analysis for the labeled *Hs*_cen1-$^{15}N_2$-Arg_{16}*Hs_Sfi1*p_{21} Complex. The third temperature range is depicted above. (A) Spectral overlay, (B) synchronous plot, (C) asynchronous plot.

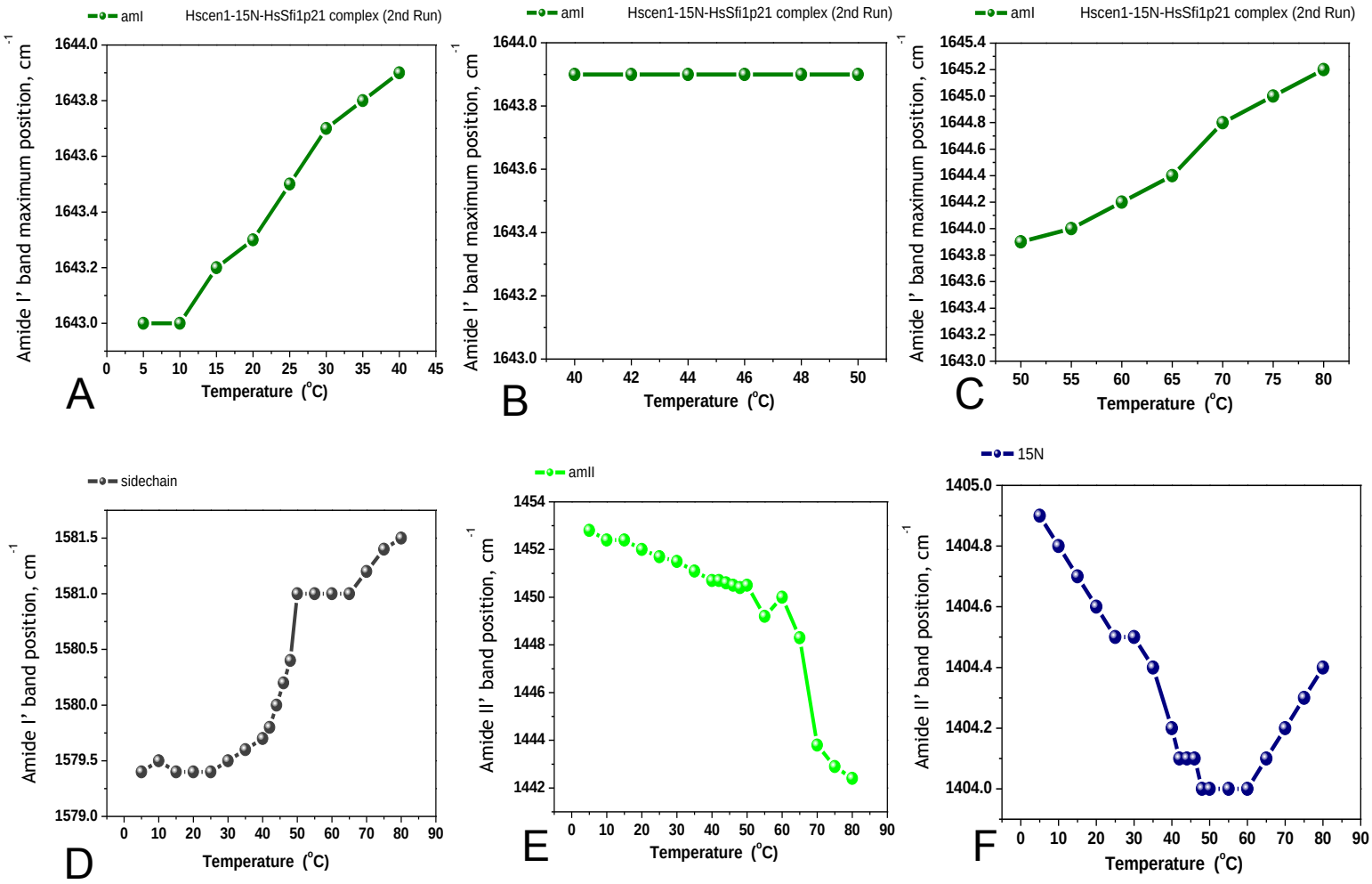

Figure 28. Temperature Dependence Plots corresponding to the Hscen1-$^{15}N_2$-Arg_{16}*Hs_Sfi1*p_{21} Complex

These plots represent the complex formation and transition of Hscen1-$^{15}N_2$-Arg_{16}*Hs_Sfi1*p_{21}. (A) and (C) represent the steps previous to and after the complex formation. (B) The complex formation has relative stability from 40°C to 50°C. (D) The peak contribution of side chain interactions shifts as the temperature increases. (E) As the temperature increases the peak contribution of the amide II' band shifts to lower wavenumbers. (F) Shift in wave number as part of the contribution of the labeled peptide.

5. CONCLUSIONS

To better evaluate the interaction between centrin and its putative novel target Krr1, a sufficient product yield and purity need to be achieved. We have successfully demonstrated the recombinant generation of novel centrin target Krr1 by evaluating different starting clones and designing a purification protocol. Our results confirm the presence of Krr1. Other centrin targets are well known, or small enough to be synthetized for experimental studies. Sfi1, though not small, is one such well known target. By isotope labeling with $^{15}N_2$ the 16^{th} arginine in *Hs_Sfi1*p_{21} we were able to demonstrate the existence of a salt bridge interaction between that residue and exposed glutamate residues of *Hs*cen1.

6. FUTURE WORK

Novel centrin target Krr1

The *E. coli* used in this study showed difficulty in expression of novel protein Krr1. To further develop the study of Krr1, we propose changing the expression strain. The sequence will be reexamined to find a suitable cloning vector and procedure. Furthermore, by evaluating the bacterial clone without a poly-A tail, the expression yield of this recombinant protein could be greatly improved.

*Hs*cen1-$^{15}N_2$-R_{16}-*Hs*_Sfi1p_{21} complex

Because 2D-IR permits the visualization of protein-protein interactions (PPI's) down to the molecular level we can clearly see the expected salt bridge interaction that occurs with the 16th Arginine residue of *Hs_Sfi1*p_{21}. As a means to advance the study of centrin and its targets, further biophysical techniques are available to assay other *Hs_Sfi1* centrin binding sites. Techniques to be explored are isothermal titration calorimetry (ITC) and further analyses with two-dimensional perturbation spectroscopy with full length version of the interacting proteins.

7. APPENDIX

7.1 APPENDIX A

QUIM 8995: BIOINFORMATICS, PROTEINS & PROTEIN-PROTEIN INTERACTIONS (PPI'S)

SEARCH PATTERN FOR KRR1 USING KNOWN CENTRIN LIGANDS

INTRODUCTION

The construction of a search pattern is a key component in revealing potential interactions between a known protein and a novel target. Using known centrin ligands[2,31,64-67] and sequence alignment tools we are able to generate a search pattern to use for comparison with the full length small subunit procesome component Krr1[45], a novel centrin target.

Known centrin ligands with their amino acid sequence:

>XPC[64]

XNWKLLAKGL LIRERLKR

>KAR1[65]

KKRELIESKW HRLLFHDKK

>Sfi1[66] peptide_2K2I

RADLHHQHSV LHRALQAWVT

>Myosin[67]

KRRWKKNFIA VSAANRFKKI SS

>XPC_2GGM[31]

NWKLLAKGLL IRERLKR

>Sfi1[2] peptide_2DOQ

GPLGSNEEAN RFANQAKLRV QEAVFYIWSD KTLKYSQMAN
DEAESFRNTW LLFRSFQQWI TLTQTFKEQS RLADQAFLNK
MFRKILKAQE HWKH

Figure A.1 ClustalW Analysis using Sfi1p_2DOQ (94 aa peptide)

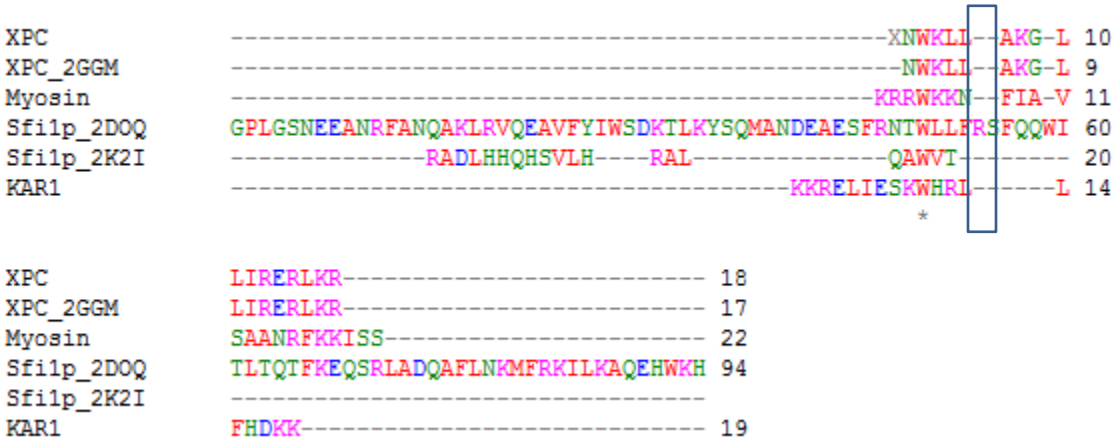

Figure A.2 Scores Table for the ClustalW analysis using Sfi1p_2DOQ

Scores Table

View Output File

SeqA	Name	Length	SeqB	Name	Length	Score
1	XPC	18	2	KAR1	19	11.0
1	XPC	18	3	Sfi1p_2K2I	20	5.0
1	XPC	18	4	Myosin	22	22.0
1	XPC	18	5	XPC_2GGM	17	100.0
1	XPC	18	6	Sfi1p_2DOQ	94	22.0
2	KAR1	19	3	Sfi1p_2K2I	20	5.0
2	KAR1	19	4	Myosin	22	5.0
2	KAR1	19	5	XPC_2GGM	17	11.0
2	KAR1	19	6	Sfi1p_2DOQ	94	5.0
3	Sfi1p_2K2I	20	4	Myosin	22	5.0
3	Sfi1p_2K2I	20	5	XPC_2GGM	17	5.0
3	Sfi1p_2K2I	20	6	Sfi1p_2DOQ	94	30.0
4	Myosin	22	5	XPC_2GGM	17	23.0
4	Myosin	22	6	Sfi1p_2DOQ	94	9.0
5	XPC_2GGM	17	6	Sfi1p_2DOQ	94	23.0

Figure A.3 Multiple Sequence Alignment without Sfi1p_2DOQ

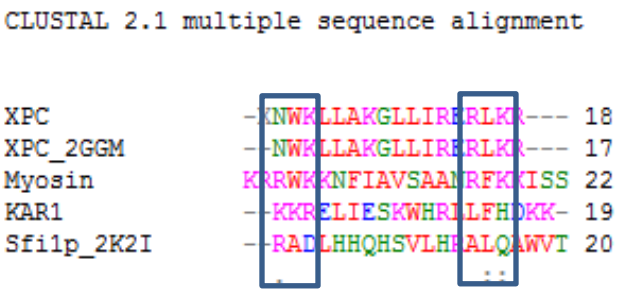

Figure A.4 Scores Table for the ClustalW analysis without Sfi1p_2DOQ

Scores Table

View Output File

SeqA	Name	Length	SeqB	Name	Length	Score
1	XPC	18	2	KAR1	19	11.0
1	XPC	18	3	Sfi1p_2K2I	20	5.0
1	XPC	18	4	Myosin	22	22.0
1	XPC	18	5	XPC_2GGM	17	100.0
2	KAR1	19	3	Sfi1p_2K2I	20	5.0
2	KAR1	19	4	Myosin	22	5.0
2	KAR1	19	5	XPC_2GGM	17	11.0
3	Sfi1p_2K2I	20	4	Myosin	22	5.0
3	Sfi1p_2K2I	20	5	XPC_2GGM	17	5.0
4	Myosin	22	5	XPC_2GGM	17	23.0

With this information the following search patterns were assayed:

a. R-XXXXXXXXXXXXXX-L/F-K NO HIT

b. R-X-K-XXXXXXXXXXXX-L/F-K NO HIT

c. R-X-L-K-XXXXXXXXXX-L/F-K NO HIT

d. R/K-W-XXXXXXXXXXXX-L/F-K NO HIT

e. [RK]-x(8)-[LW] 8 HITS

Figure A.5 Search Pattern Hits using the last search pattern

Hits for USERPAT1{[RK]-x(8)-[LW]} motif on sequence USERSEQ1 :

found: 8 hits in 1 sequence

USERSEQ1 (381 aa)

```
MASPSLERPEKGAGKSEFRNQKPKPENQDESELLTVPDGWKEPAFSKEDNPRGLLEESSFATLFPK
YREAYLKECWPLVQKALNEHHVNATLDLIEGSMTVCTTKKTFDPYIIIRARDLIKLLARSVSFEQA
VRILQDDVACDIIKIGSLVRNKERFVKRRQRLIGPKGSTLKALELLTNCYIMVQGNTVSAIGPFSG
LKEVRKVALDTMKNIHPIYNIKSLMIKRELAKDSELRSQSWERFLPQFKHKNVNKRKEPKKKTVKK
EYTPFPPPQPESQIDKELASGEYFLKANQKKRQKMEAIKAKQAEAISKRQEERNKAFIPPKEKPIV
KPKEASTETKIDVASIKEKVKKAKNKKLGALTAEEIALKMEADEKKKKKKK
```

hits by patterns: [8 hits (by 1 pattern) on 1 sequence]

Hits by **USERPAT1** :
Pattern: **[RK]-x(8)-[LW]**
Approximate number of expected random matches [Ref: PMID 11535175] in ~ 100'000 sequences (50'000'000 residues): 548083

USERSEQ1  (381 aa)

24 - 33:	KpenqdeseL
163 - 172:	RligpkgstL
168 - 177:	KgstlkaleL
225 - 234:	KrelakdseL
230 - 239:	KdselrsqsW
280 - 289:	KelasgeyfL
349 - 358:	KvkkaknkkL
352 - 361:	KaknkklgaL

The above figure indicates that eight matches for potential sites of interaction were found in the total sequence.

[Summary of Results and Conclusions]

Four different search patterns were generated using six known centrin targets; however none of the patterns produced a hit in the Krr1 sequence. In a final attempt, a fifth, more generalized pattern was generated using as a basis the conserved tryptophan residue. This last search pattern indicated eight total hits within the protein sequence. These hits reveal a potential binding site for centrin within the Krr1 sequence.

8. REFERENCES

1. Kilmartin, J. V. Sfi1p has conserved centrin-binding sites and an essential function in budding yeast spindle pole body duplication. *J. Cell Biol*. **2003**. 162(7), 1211-1221.

2. Li, S.; Sandercock, A.L.; Conduit, P.; Robinson, C.V.; Williams, R.L.; Kilmartin, J.V. Structural role of Sfi1p-centrin filaments in budding yeast spindle pole body duplication. *J Cell Biol*. **2006**. 173(6): 867–877.

3. Kim, J.J.; Rajagopalan, K.; Hussain, B.; Williams, B.H.; Kulkarni, P.; Mooney, S.M. CETN1 is a cancer testis antigen with expression in prostate and pancreatic cancers. *Biomarker Res*. **2013.** 1:22.

4. Noda, I. Recent advancement in the field of two-dimensional correlation spectroscopy. *J. Mol. Struct*. **2008.**(883–884): 2-26.

5. Kellogg, D. R., Moritz, M.; Alberts, B. M. The centrosome and cellular organization. *Annu. Rev. Biochem*. **1994**. *63*(1), 639-674.

6. Bornens, M. The centrosome in cells and organisms. *Science*. **2012**. 335, 422-426.

7. Bettencourt-Dias, M.; Glover, D. M. Centrosome biogenesis and function: centrosomics brings new understanding. *Nat. Rev. Mol. Cell Biol*. **2007** 8(6), 451-463.

8. Adams, I. R.; Kilmartin, J. V. Spindle pole body duplication: a model for centrosome duplication?. *Trends Cell Biol*. **2000.** 10(8), 329-335.

9. Alverts, B.; Johnson, A.; Lewis, J.; Raff, M.; Roberts, K.; Walter, P. In *Molecular Biology of the Cell,* 5th Ed; Garland Science: New York, NY, **2008**, 992-994.

10. Kim, J. C., Badano, J. L., Sibold, S., Esmail, M. A., Hill, J., Hoskins, B. E.; Beales, P. L. The Bardet-Biedl protein BBS4 targets cargo to the pericentriolar region and is required for microtubule anchoring and cell cycle progression. *Nat.Genet*. **2004** 36(5), 462-470.

11. Pearson, C. G.; Bloom, K. Dynamic Microtubules Lead the Way for Spindle Positioning. *Nat. Rev. Mol. Cell Biol*. **2004**. 5, 481-492.

12. Feldman, J. L., Geimer, S., & Marshall, W. F. The mother centriole plays an instructive role in defining cell geometry. PLoS Biol. **2007**. 5(6), 149.

13. Pihan, G. A. Centrosome Dysfunction Contributes to Chromosome Instability, Chromoanagenesis, and Genome Reprograming in Cancer. *Front Oncol*. **2013**(3): 277.

14. Kuriyama, R.; Borisy, G. G. Centriole cycle in Chinese hamster ovary cells as determined by whole-mount electron microscopy. *J. Cell Biol*. **1981**. 91, 814–821.

15. Azimzadeh, J., & Bornens, M. Structure and duplication of the centrosome. *J. Cell Sci*. **2007**. 120(13), 2139-2142.

16. Jaspersen, Sue L., and Tim Stearns. Exploring the pole: an EMBO conference on centrosomes and spindle pole bodies. *Nat. Cell Biol*. **2008**. (10)12:1375.

17. Salisbury, J. L., Suino, K. M., Busby, R., & Springett, M. Centrin-2 is required for centriole duplication in mammalian cells. *Current Biology*. **2002**.12(15), 1287-1292.

18. Jana, S. C., Marteil, G., & Bettencourt-Dias, M. Mapping molecules to structure: unveiling secrets of centriole and cilia assembly with near-atomic resolution. *Curr. Opin. Cell Biol*.**2014**. 26: 96-106.

19. Bettencourt-Dias, M., Hildebrandt, F., Pellman, D., Woods, G., & Godinho, S. A. Centrosomes and cilia in human disease. *Trends in Genetics*. **2011**. 27(8), 307-315.

20. Basto, R., Brunk, K., Vinadogrova, T., Peel, N., Franz, A., Khodjakov, A., & Raff, J. W. Centrosome amplification can initiate tumorigenesis in flies. *Cell*. **2008**. 133(6), 1032-1042.

21. Boveri, T. Concerning the origin of malignant tumours by Theodor Boveri. Translated and annotated by Henry Harris *J. Cell Sci.* **2008.** (121): 1–84.

22. Nigg, E. A.; Raff, J.W. Centrioles, Centrosomes, and Cilia in Health and Disease. *Cell*. **2009.** (139): 663–678.

23. Kobayashi, T., & Dynlacht, B. D. Regulating the transition from centriole to basal body. *J. Cell Biol*. **2011**. 193(3), 435-444.

24. Salisbury, J.L. Centrin, centrosomes, and mitotic spindle poles. *Curr. Opin. Cell Biol*. **1995.** (*7)*:39–45.

25. Salisbury, J.L. A mechanistic view on the evolutionary origin for centrin-based control of centriole duplication. *J. Cell. Phys.* **2007**. 213(2):420-428.

26. Jerka-Dziadosz, M., Koll, F., Włoga, D., Gogendeau, D., Garreau de Loubresse, N., Ruiz, F. & Beisson, J. A Centrin3-dependent, Transient, Appendage of the Mother Basal Body Guides the Positioning of the Daughter Basal Body in *Paramecium*. *Protist*. **2013**. 164(3), 352-368.

27. Resendes K.K.; Rasala B.A., and Forbes D.J. Centrin 2 Localizes to the Vertebrate Nuclear Pore and Plays a Role in mRNA and Protein Export. *Mol. Cell. Biol.* **2008.** 28(5),1755-1769.

28. Errabolu, R., Sanders, M.A., and Salisbury, J.L. Cloning of cDNA encoding human centrin, an EF-hand protein of centrosomes and mitotic spindle poles. *J. Cell Sci.* **1994**. 17, 9-16.

29. Wolfrum, U., and Salisbury, J.L. Expression of centrin isoforms in the mammalian retina. *Experimental Cell Research*. **1998**. 242, 10-17.

30. Dantas, T.; Wang, Y.; Lalor, P.; Dockery, P.; Morrison, C. *J. Cell Biol*. **2011** 193, 307–318.

31. Thompson, J. R., Ryan, Z. C., Salisbury, J. L., & Kumar, R. The structure of the human centrin 2-xeroderma pigmentosum group C protein complex. *J. Biol. Chem.* **2006**. 281(27), 18746-18752.

32. Gavet O., Alvarez C., Gaspar P., Bornens M. Centrin4p, a novel mammalian centrin specifically expressed in ciliated cells. *Mol. Biol. Cell* **2003.** 14:1818-1834.

33. Giessl A., Pulvermuller A., Trojan P., Park J.H., Choe H.W., Ernst O.P., Hofmann K.P., Wolfrum U. Differential expression and interaction with the visual G-protein transducin of centrin isoforms in mammalian photoreceptor cells. *J. Biol. Chem.* **2004**. 279:51472-5148.

34. Jani, D.; Lutz, S.; Marshall, N. J.; Fischer, T.; Köhler, A.; Ellisdon, A. M.; Hurt, E.; Stewart, M. Sus1, Cdc31, and the Sac3 CID region form a conserved interaction platform that promotes nuclear pore association and mRNA export. Mol.Cell. **2009.** 33(6), 727-737.

35. Sosa, L. D. V.; Alfaro, E.; Santiago, J.; Narváez, D.; Rosado, M. C.; Rodríguez, A.; Gomez, A.M.; Schreiter, E.R.; Pastrana-Ríos, B. The structure, molecular dynamics, and energetics of centrin–melittin complex. *Proteins*. **2011.** 79(11), 3132-3143.

36. Pastrana-Rios, B.; Ocaña, W.; Rios, M.; Lorenzo Vargas, G.; Ysa, G.; Poynter, G.; Tapia, J.; Salisbury, J.L. Centrin: its secondary structure in the presence and absence of cations. *Biochemistry*. **2002**. 41 (22):6911–6919.

37. Pastrana-Ríos, B.; Reyes, M.; De Orbeta, J.; Meza, V.; Narváez, D.; Gómez, A. M.; Rodríguez Nassif, A.; Almodóvar, R.; Díaz Casas, A.;Robles, J.; Ortiz, A.M.; Irizarry, L.; Campbell, M.; Colón, M. Relative Stability of Human Centrins and Its Relationship to Calcium Binding. *Biochemistry*. **2013.** 52(7): 1236-1248.

38. Rafelski, S. M., Keller, L. C., Alberts, J. B., & Marshall, W. F. Apparent diffusive motion of centrin foci in living cells: implications for diffusion-based motion in centriole duplication. *Phys. Biol*. **2011**. 8(2), 026010.

39. Azimzadeh, J. & Bornens, M. in Centrosomes in Development and Disease (ed. Nigg, E. A.) 93–122 (Wiley-Vch, Weinheim, **2004**).

40. Salisbury, J.L. Centrosomes: Sfi1p and centrin unravel a structural riddle. *Current Biology*. **2004.** 14, R27-R29.

41. Kilmartin, J.V. Genetic and biochemical approaches to spindle function and chromosome segregation in eukaryotic microorganisms. *Curr. Opin. Cell Biol*. **1994**. 6, 50–54.

42. Anderson, V. E., Prudden, J., Prochnik, S., Giddings, T. H., & Hardwick, K. G. Novel sfi1 alleles uncover additional functions for Sfi1p in bipolar spindle assembly and function. *Mol. Biol. Cell*. **2007**. 18(6), 2047-2056.

43. Martinez-Sanz, J., Yang, A., Blouquit, Y., Duchambon, P., Assairi, L., & Craescu, C. T. Binding of human centrin 2 to the centrosomal protein hSfi1. *FEBS J.* **2006**. 273(19), 4504-4515.

44. Kilmartin, J. V. Lessons from yeast: the spindle pole body and the centrosome. *Philos. Trans. R. Soc. London, Ser. B.* **2014**. 369(1650), 20130456.

45. Bernstein K.A.; Gallagher J.E., and Mitchell B.M., Granneman S., Baserga S.J. The small-subunit processome is a ribosome assembly intermediate. *Euk. Cell.* **2004**. 1619–1626.

46. Scherl, A.; Coute, Y.; Deon, C.; Calle, A.; Kindbeiter, K.; Sanchez, J.C.; Greco, A.; Hochstrasser, D.F.; Diaz, J.J. Functional proteomic analysis of human nucleolus. *Mol. Biol. Cell.* **2002**. 13, 4100-4109.

47. Universal Protein Resource (UniProt), UniProt Knowledgebase (UniProtKB)UniProtKB/Swiss-Prot Q13601 (KRR1_HUMAN) http://www.uniprot.org/uniprot/Q13601#ref3 (**Accessed June 2010**)

48. Sasaki, T.; Toh-e, A.; Kikuchi, Y. Yeast Krr1p physically and functionally interacts with a novel essential Kri1p, and both proteins are required for 40S ribosome biogenesis in the nucleolus. *Mol. Cell. Biol.* **2000**. 20, 7971-7979.

49. Siomi, H.; Choi, M.; Siomi, M.C.; Nussbaum, R.L.; Dreyfuss, G. Essential role for KH domains in RNA binding: Impaired RNA binding by a mutation in the KH domain of FMR1 that causes fragile X syndrome. *Cell.* **1994.** 77(1):33–39.

50. Golebiowski, F., Matic, I., Tatham, M.H., Cole, C., Yin, Y., Nakamura, A., Cox, J., Barton, G.J., Mann, M. Hay, R.T. System-wide changes to SUMO modifications in response to heat shock. *Sci Signal.* **2009**.

51. Sowa, ME, Bennett, EJ, Gygi, SP, Harper, JW. Defining the human deubiquitinating enzyme interaction landscape. *Cell.* **2009**. 389-403.

52. Byler, D.M.; Susi, H. Examination of the secondary structure of proteins by deconvolved FTIR spectra. *Biopolymers*. **1986**. 25:469-487.

53. Surewicz, W.K.; Mantsch, HH. Determination of protein secondary structure by Fourier transform infrared spectroscopy: a critical assessment. *Biochim. Biophys. Acta* **1988**. 952:115-130.

54. Kunihiro, K.; Kim, P. and Baldwin, R.L. Strategy for trapping intermediates in the folding of ribonuclease and for using 1H-NMR to determine their structures. *Biopolymers* **1984**. 22:59-67

55. DeFlores, L.P.; Ganim Z., Nicodemus R.A. and Tokmakoff A. Amide I′−II′ 2D IR Spectroscopy Provides Enhanced Protein Secondary Structural Sensitivity. *J. Am. Chem. Soc*. **2009**. 131(9):3385–3391.

56. Pastrana-Ríos, B. Mechanism of unfolding of a model helical peptide. *Biochemistry*. **2001**. 40(31): 9074-9081.

57. Pastrana-Ríos, B. Simulation of FT-IR spectra and 2D-COS analysis for thethermal perturbation of apo-centrin. *J. Mol. Struct*. **2006.** 799.1,163-167.

58. Ocaña, W. and Pastrana-Ríos, B. Calcium titration of *Chlamydomonas reinhartii* centrin and its structural changes. *J. Mol. Struct*. **2014**. 1069, 73-78.

59. Pastrana-Ríos, B. Thermal perturbation correlation of calcium binding Human centrin 3 and its structural changes. *J. Mol. Struct*. **2014**. 1069, 85-88.

60. Noda, I. Recent developments in two-dimensional (2D) correlation spectroscopy. *Chin. Chem. Lett*. **2014**. 26(2): 167–172.

61. Pastrana-Rios, B., Iloro-Manzano , I. United States Patent US 8,268,628 B1 (18 September 2012)

62. Refaeli, B.; Goldbourt, A. Protein expression and isotopic enrichment based on induction of the Entner-Doudoroff pathway in Escherichia coli. *Biochem Biophys Res Commun*. **2012**. 427(1):154-158.

63. Pall Corporation Acrosep™ 1 mL Pre-Packed Chromatography Columns http://www.pall.com/pdfs/Laboratory/1273_89127A_nc.pdf (**Accessed September 2010**)

64. Charbonnier, J. B;, Renaud, E., Miron, S.; Le Du, M. H.; Blouquit, Y.; Duchambon, P.; Christova, P.; Shosheva, A.; Rose, T.; Angulo, J.F.; Craescu, C. T. Structural, thermodynamic, and cellular characterization of human centrin 2 interaction with xeroderma pigmentosum group C protein. *J.Mol.Biol*. **2007**. *373*(4), 1032-1046. [PDB ID 2OBH]

65. Hu, H.; Chazin, W. J. Unique features in the C-terminal domain provide caltractin with target specificity. *J.Mol.Biol*. **2003**. 330(3), 473-484. [PDB ID 1OQP]

66. Martinez-Sanz, J.; Kateb, F.; Assairi, L.; Blouquit, Y.; Bodenhausen, G.; Abergel, D.; Mouawad, L.; Craescu, C. T. Structure, dynamics and thermodynamics of the human centrin 2/hSfi1 complex. *J.Mol.Biol*. **2010.** 395(1), 191-204. [PDB ID 2K2I]

67. Radu, L.; Miron, S.; Durand, D.; Assairi, L.; Blouquit, Y.; Charbonnier, J.B. Structural features of the complexes formed by Scherffelia dubia centrin. Journal: To be Published [PDB ID 3KF9]